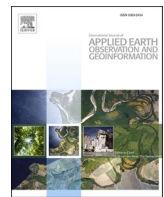




Contents lists available at ScienceDirect

International Journal of Applied Earth Observations and Geoinformation

journal homepage: www.elsevier.com/locate/jag



Trail camera networks provide insights into satellite-derived phenology for ecological studies

Nanfeng Liu ^{a,*}, Matthew Garcia ^a, Aditya Singh ^b, John D.J. Clare ^a, Jennifer L. Stenglein ^c, Benjamin Zuckerberg ^a, Eric L. Kruger ^a, Philip A. Townsend ^a

^a Department of Forest and Wildlife Ecology, University of Wisconsin-Madison, United States

^b Department of Agricultural and Biological Engineering, University of Florida, United States

^c Wisconsin Department of Natural Resources, United States



ARTICLE INFO

Keywords:

Phenology
Trailcam
Understory
Harmonized Landsat Sentinel-2
MODIS

ABSTRACT

Repeat digital photography at or near ground-level is a proven and efficient approach for tracking plant phenology. Here, we explored the potential to monitor phenology using the Snapshot Wisconsin (SW) trail camera network, a citizen science program. Using three curve-fitting methods for characterizing phenological transition dates, we assessed the phenological offset between understory vegetation and the overstory canopy in the trailcam observations and compared variations in derived phenology over the different spatial scales represented by trailcams (~20–50 m), Harmonized Landsat and Sentinel-2 (HLS, 30 m), and Moderate Resolution Imaging Spectroradiometer (MODIS, 500 m). Our results showed that the apparent phenological offset between understory and overstory vegetation differed among forest types: in broadleaf deciduous forests, understory vegetation had an earlier start-of-spring (SOS) and later end-of-autumn (EOA) than the overstory canopy; in mixed forests, the understory showed an earlier SOS than the overstory, but no significant difference in EOA; in evergreen conifer forests, neither SOS nor EOA differed significantly between the understory and overstory. We found moderate correlations ($0.25 \leq r \leq 0.57$) between trailcam- and satellite-derived phenological dates. Moreover, those derived dates varied significantly among the applied curve-fitting methods: total growing season length (from SOS to EOA) could be 19 days longer for a threshold-based method than for a logistic curve-fitting method (our reference model), but 17 days shorter than the logistic method when using a piecewise-continuous method based on fitted sine curves. Despite the spatial limitations of trailcams for characterizing phenology on landscape and regional scales, trailcam networks have considerable potential for informing local phenological studies and disentangling the many drivers of phenology that can remain undetected from the satellite perspective.

1. Introduction

The timing of biological events during the annual growth cycle such as budburst and leaf expansion, flowering and fruiting, and leaf senescence and abscission are generally referred to as plant phenology. In a given year, the phenological progression is a valuable diagnostic of vegetation processes in ecosystems and their response to weather, especially temperature and moisture availability. Over medium to long time scales, changes in phenology may be associated with climate change (Monahan et al., 2016; Schwartz et al., 2006; Wolkovich et al., 2012). For example, increased late winter and spring temperatures can advance spring phenology in temperate regions, but may have variable

effects on autumn senescence (Badeck et al., 2004; Chmielewski and Rötzer, 2001; Cleland et al., 2007; Peñuelas, 2001; Walther et al., 2002). Climate-driven shifts in the timing of phenological events can, in turn, have both positive and negative feedbacks on that climate change (Desai, 2010). Through photosynthesis, carbon sequestration, and transpiration, vegetation phenology is a primary component in the intertwined exchanges of energy, carbon and water at the land surface (Peñuelas et al., 2009; Richardson et al., 2013).

Traditional monitoring of phenology requires in-situ observers to record the timing of specific biological events such as budburst, flowering or fruiting (Haggerty and Mazer, 2008). In the past decades, several observation networks such as the USA National Phenology

* Corresponding author.

E-mail address: nliu58@wisc.edu (N. Liu).

Network (NPN) (Elmendorf et al., 2016; Schwartz et al., 2012) and the European Phenology Network (EPN) (van Vliet et al., 2003) have been established, with these networks located primarily in temperate (*i.e.*, seasonal) ecosystems. A disadvantage of individual-based networks is that the observations, even as a collection, do not often describe phenological patterns across the landscape that result from varying species mixtures and from environmental gradients in soil types, topography and microclimate variability.

To extend this paradigm, satellite-based remote sensing provides an opportunity for observing phenology at large scales and over increasingly longer time periods. Various phenological analyses have used NASA/USGS Landsat missions with 30-m pixels (Dong et al., 2015; Fisher et al., 2006; Melaas et al., 2016b, 2013; Nijland et al., 2016; Walker et al., 2012), NASA EOS Moderate Resolution Imaging Spectroradiometer (MODIS) with pixel sizes from 250 m to 1 km (Fisher and Mustard, 2007; Ganguly et al., 2010; Sakamoto et al., 2005; White et al., 2009; Zhang et al., 2003), and ESA Sentinel-2 missions with 10-m pixels (Melaas et al., 2016b; Vrieling et al., 2018). Ongoing work addresses uncertainties in observations due to sensor calibration, atmospheric effects, cloud contamination, and bidirectional reflectance distribution function (BRDF) effects (Fisher and Mustard, 2007; Zheng and Zhu, 2017).

Repeat digital photography at or near the ground has been demonstrated as a useful tool for monitoring plant phenology (Brown et al., 2016) and is one of the principal methods by which the satellite-based observations can be validated directly. By tracking color changes in digital images, the timing of key phenology stages such as leaf growth, flowering, and senescence can be identified. Unlike traditional field observations, and depending on their point of view, “phenocameras” can capture phenology over areas from $\sim 10 \text{ m}^2$ to a hectare or more, helping bridge the spatial gap between traditional ground- and satellite-based observations. A number of phenocamera networks have been established worldwide: PhenoCam in North America (Richardson et al., 2018a,b), EuroPhen in Europe (Wingate et al., 2015), PEN (Phenological Eyes Network) in Japan (Nasahara and Nagai, 2015), and APN (Australian Phenocam Network) in Australia (Moore et al., 2016). These data have been widely used to validate satellite-derived phenology (Hufkens et al., 2012; Klosterman et al., 2014; Melaas et al., 2016a,b; Richardson et al., 2018a,b), a practice now common enough that several software packages have been developed for community use in pre-processing and extracting phenology information from phenocamera or satellite images (*e.g.*, Phenopix, Filippa et al., 2016; Phenocamr, Hufkens et al., 2018, and TIMESAT, Eklundh and Jönsson, 2016).

Methods for deriving phenological metrics from time-series data, such as the start and end of the growing season, can generally be divided into two categories: (1) those based on specific thresholds in the filtered time series, or (2) those based on inflection points in smooth curves fitted to the time series. For the first method, a set of local or global functions is often applied to the time series for noise reduction as by median smoothing (Reed et al., 1994), moving average (White et al., 2009), Savitzky-Golay filter (Chen et al., 2004), local splines (Richardson et al., 2018a,b) and double logistic functions (Beck et al., 2006; Zhang et al., 2003). Pre-defined thresholds are then identified in the smoothed time series to determine the dates when phenological transitions are assumed to occur (Myneni et al., 1997; Richardson et al., 2018a,b). The second method fits time series data with global functions, such as the commonly used logistic function (Beck et al., 2006; Zhang et al., 2003), an asymmetric Gaussian function (Jonsson and Eklundh, 2002) or a harmonic function (Moody and Johnson, 2001). Phenological transition dates are then determined by identifying the extrema and inflections of the fitted curves and their derivatives.

Here we assess the potential for using image time series from a network of trail cameras (“trailcams”) to characterize phenology. Trailcams differ from phenocameras in design, cost, objective, use, and placement. Trailcams are typically used by citizens, researchers, and wildlife agencies to track animal activity (Steenweg et al., 2017) and are

thus a potentially rich resource for monitoring vegetation, especially if programmed to obtain dedicated photos at a common time each day to generate time lapse sequences. Because of their placement, usually at about 0.75–1.0 m above the ground, trailcams provide a unique perspective on both overstory and understory phenology, which generally remain indistinct in most phenocam- and satellite-based analyses (but see St. Peter et al., 2018).

The Snapshot Wisconsin (SW) trailcam network used in this study is a citizen science effort: cameras provided by the Wisconsin Department of Natural Resources are placed on both public and private lands, ensuring wider and more diverse spatial coverage than networks that may be restricted to public lands alone. Snapshot Wisconsin is a broad scale citizen science and crowdsourcing effort to deploy more than 2000 motion-triggered trailcams in natural ecosystems, primarily forest areas, across Wisconsin with an ultimate goal density of one camera per 23.3 km^2 (9 mi^2 , equivalent to a quarter-township in the US Public Land Survey System). An overall objective of SW is to link wildlife observations via trailcams with satellite-based observations of vegetation phenology, productivity, composition, and fragmentation to aid analysis and prediction of wildlife distributions, community composition, and behavior in space and time (Clare et al., 2019; Locke et al., 2019; Townsend et al., in review). A key objective of continuously operating trail cameras is to observe how animal occurrence and behavior vary seasonally, and in conjunction with seasonal variation in vegetation density and vigor that provide wildlife forage and shelter resources (Townsend et al., in review).

The SW cameras provide a unique daily record with photos of vegetation recorded at 10:40 AM local time each day, regardless of wildlife activity, that can be used to understand and validate phenological interpretations from satellite imagery. In this study, we used a preliminary set of SW time-lapse images to compare interpretations of phenology from satellite remote sensing with those derived from daily trailcam photos. We linked a unique combination of datasets to address three questions. First, are the derived and extracted phenological transition dates for a given location consistent across the available trailcam and satellite data sources? Second, to what extent can each data source used here (trailcams, HLS, and MODIS images) detect local differences between understory and overstory green-up and senescence dates? Finally, do different methods used to extract phenological transition dates from the trailcam time series lead to systematic differences between their results?

2. Study sites

Snapshot Wisconsin covers the state of Wisconsin (longitude -86.25 to -93.14°W , latitude 42.30 – 47.17°N), USA (Fig. 1). Elevation ranges from 177 m ASL along the Lake Michigan shore to 595 m in north central Wisconsin. The statewide annual temperature (from 1971 to 2000) averages 6.2°C , with the lowest monthly temperature (-10.4°C) in January in the northwest and the highest (20.6°C) in August in the south. The average annual precipitation in Wisconsin is 830 mm, with the lowest monthly precipitation (30 mm) in January and the highest (110 mm) in August (<http://www.aos.wisc.edu/~sco/>). The growing season typically extends 4–6 months (May through October) with earlier springs being observed as climate has generally warmed across Wisconsin and the midwestern US over the past 30 years (Schwartz et al., 2006; Morin et al., 2009; Serbin and Kucharik, 2009; Jeong et al., 2011; Ault et al., 2015; Garcia and Townsend, 2016).

Land cover in Wisconsin is $\sim 39\%$ forested land (6.7 million ha), with most of that forest area occurring in the northern half of the state (Fig. 1, Wisland 2.0 land cover map from <https://dnr.wi.gov/maps/WISCLAND.html>). Wisconsin crosses distinct ecotones between central mixed hardwoods, savanna and sub-boreal forests. As such, the types of forests are widely varied: (1) evergreen needleleaf forest in the north, dominated primarily by *Picea mariana* (black spruce) and *P. glauca* (white spruce) with *Abies balsamea* (balsam fir), *Pinus strobus* (white

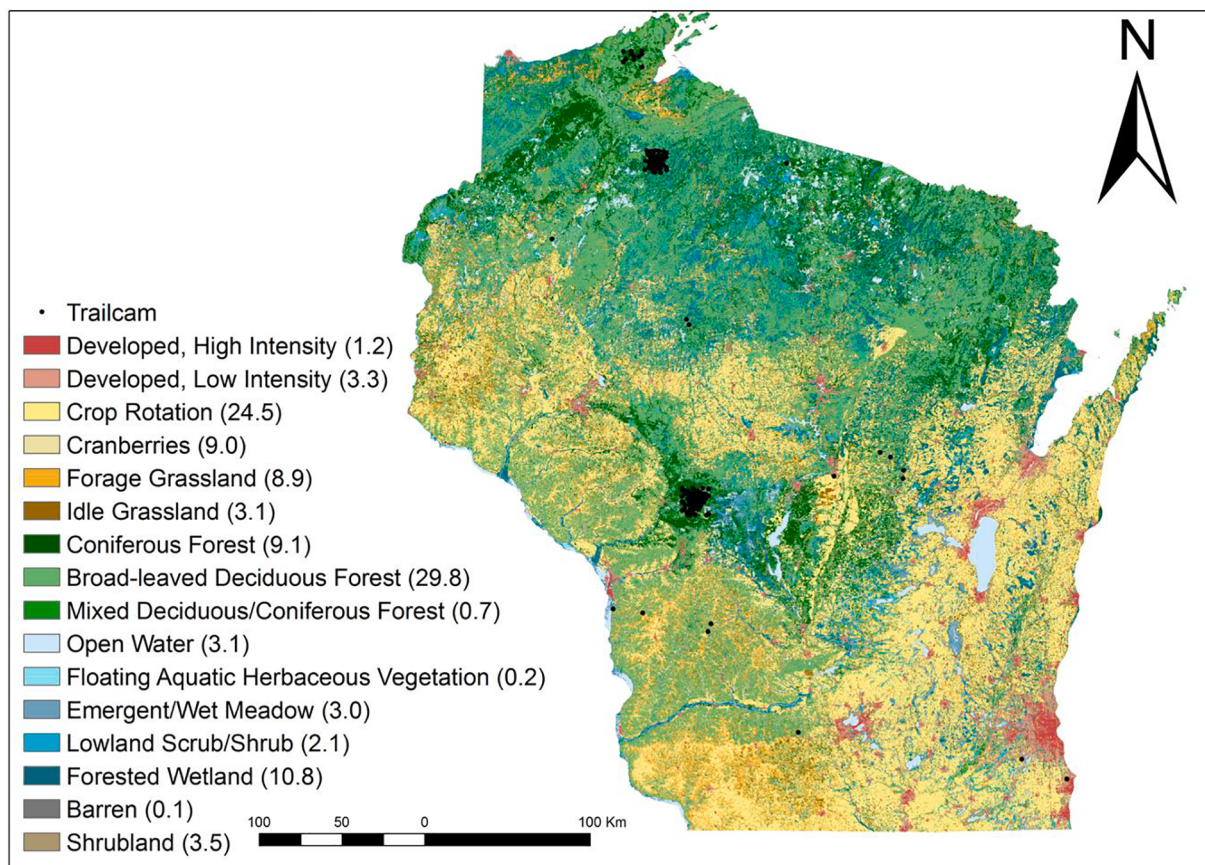


Fig. 1. Trail camera locations from 2015 to 2017 used in the analysis. Values in parentheses are the percentages of area covered by land cover type according to Wiscland 2.0.

pine), *P. resinosa* (red pine), and *P. banksiana* (jack pine); (2) deciduous broadleaf forest commonly dominated by a variety of oaks (*Quercus* spp.) in the south and west and in the north by *Populus tremuloides* (quaking aspen) and hardwoods including *Acer saccharum* (sugar maple), *Fraxinus americana* (white ash), *Tilia americana* (basswood), *Betula alleghaniensis* (yellow birch), and *A. rubrum* (red maple); and (3) areas of mixed deciduous/evergreen forest throughout the state.

3. Data and methods

3.1. Trail camera images

Snapshot Wisconsin is a volunteer-based citizen science project for monitoring wildlife populations across the state through the use of motion-activated trail cameras. Between 2015 and fall 2020, more than 1800 volunteers have been enrolled to deploy and maintain more than 2000 cameras in Wisconsin (Townsend et al., in review). The trailcams (Bushnell® Trophy Cam, 35° field-of-view in RGB channels) were mounted on mature trees approximately 1 m above the ground, facing north if possible. This setting allowed cameras to capture a wide variety of wildlife activity as well as the conditions of both understory vegetation and the lower/middle parts of overstory canopies. When motion is detected, as for animal movement within the field of view (FOV), the cameras are triggered to take sequential images. The images are then uploaded by citizen scientists to the SW database and the animals appearing in the images are identified through a variety of classification approaches, including crowdsourcing (Clare et al., 2019). In addition to motion-triggered images, each camera is programmed to collect one dedicated image daily at 10:40 am local time from which we have constructed the phenological time series for this study.

The SW camera network is being rolled out over several years due to the large number of cameras required and considerable investment for camera acquisition and citizen training. In addition, the time between photo acquisition and upload may delay photo availability up to 6 months. Due to these and other technical issues (e.g., battery failure, instrument malfunction), not all cameras capture a full phenological cycle time-series for the early SW (2015–2017) project period. In addition, some cameras experienced positional shifts such that not all cameras provided continuous images for a consistent FOV. In this study, we use daily image time series from 191 cameras in operation during 2015–2017 to construct the phenological curves in our analyses. To deal with cameras with less than a full annual phenological cycle, we divided the data into approximate half-years (days 1–200 and 200–365) to analyze spring and autumn phenology separately.

Based on camera images, we visually classified the overstory canopy into three forest types: (1) needleleaf evergreen forest; (2) broadleaf deciduous forest; (3) mixed forest. The understory vegetation was generally a mixture of shrubs, forbs, and graminoids. Preprocessing of imagery entailed first manually delineating regions of interest (ROIs) for overstory and understory canopies on each image (Fig. 2), after which the average RGB digital number (DN) values within each ROI were extracted for construction of data time series. Outlier images were then excluded, most commonly due to blurring caused by condensation on the camera lens. Under- and overexposed images due to variable scene illumination were excluded following Richardson et al. (2018):

$$DN_{red,ROI} + DN_{green,ROI} + DN_{blue,ROI} \begin{cases} < 100, \text{underexposed} \\ > 600, \text{overexposed} \end{cases} \quad (1)$$

where DN_{red} , DN_{green} , and DN_{blue} are the detector response values (range 0–255) in the trailcam image RGB channels, respectively. An example

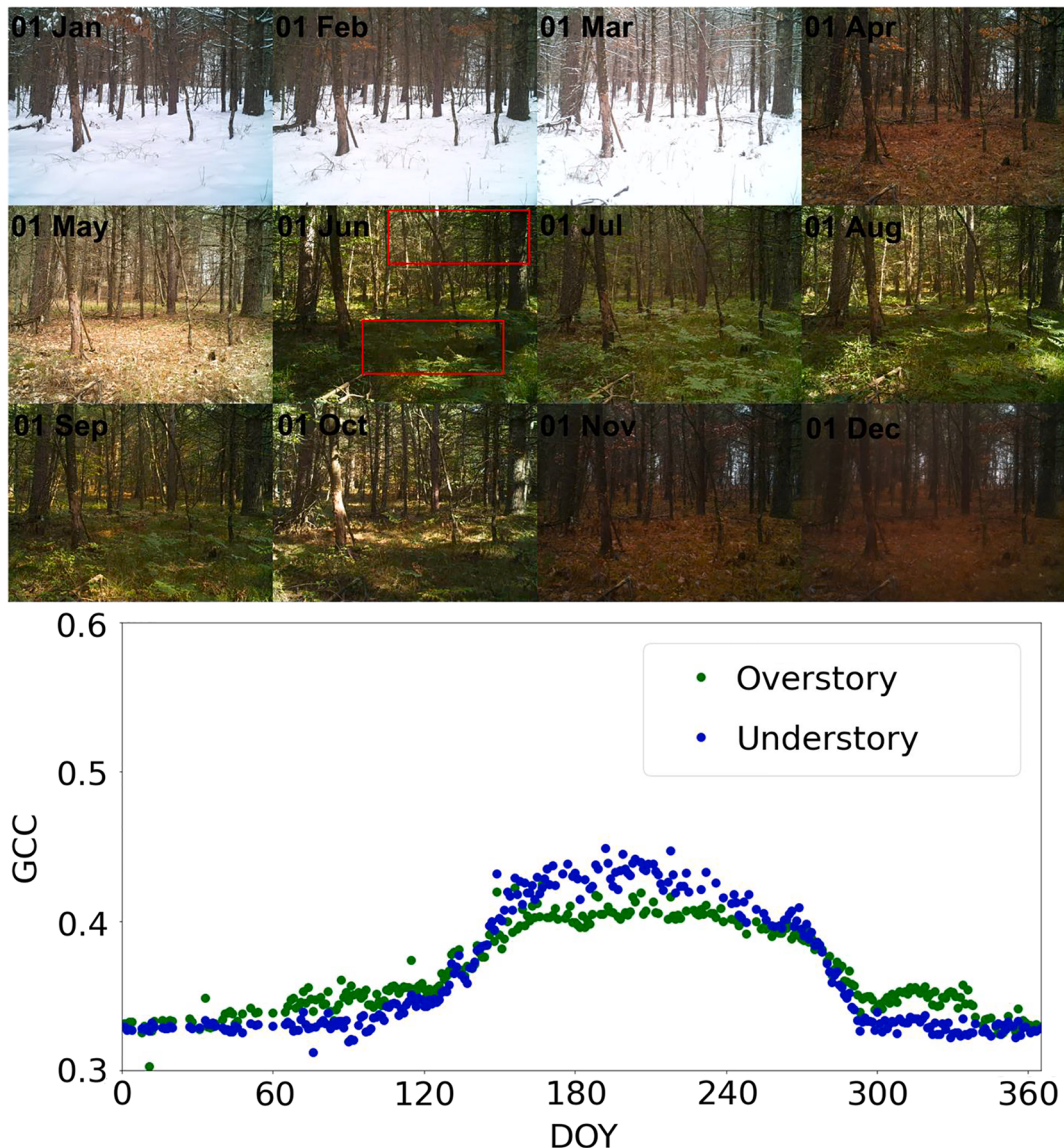


Fig. 2. Example time series of trailcam images on sampled dates for 2017 and the extracted daily GCC time series (Eq. (2)). White boxes in the June image illustrate the placement of ROIs for extraction of understory vegetation and overstory canopy GCC values.

image time series for the first day of each month throughout the year (Fig. 2) illustrates the delineation of understory and overstory ROIs, for which we then calculated the green chromatic coordinate (GCC; Richardson et al., 2018a,b):

$$GCC = \frac{DN_{green}}{DN_{red} + DN_{green} + DN_{blue}} \quad (2)$$

Fig. 2 also demonstrates an example of the GCC timeseries of understory vegetation and overstory canopy at this trailcam location. For more examples, please refer to Supplementary Fig. S-1.

3.2. Remote sensing data

3.2.1. HLS and supplemental Landsat-7 images

The NASA harmonized Landsat–Sentinel (HLS; Claverie et al., 2018) surface reflectance dataset integrates the reflectance products from the Landsat-8 Operational Land Imager (OLI, 16-day repeat cycle) and the Sentinel-2 (A and B, 10-day repeat cycle) Multi-Spectral Instrument (MSI) sensors to produce three surface reflectance products: S10, L30 and S30. The S10 product is derived from the Sentinel-2 L1C reflectance dataset and has eleven spectral bands with varying spatial resolutions:

10 m, 20 m and 60 m. The S30 product is derived from the S10 product by spectral adjustment (using Sentinel-2 bands 1–4 and 9–11) and then spatial resampling to the characteristics of the Landsat-8 OLI sensor at 30-m pixel resolution. The L30 product consists of the surface reflectance derived from the Landsat-8 L1T product, which is regridded to the Sentinel-2 tiling scheme. Both S30 and L30 are then delivered as nadir-view BRDF-adjusted surface reflectance (NBAR) products to aid in the generation of consistent observation time series. We thus used the multispectral S30 and L30 pixels at each trailcam location to extract band values and determine HLS-based phenological transition dates.

The QA layer provided in each of the two products was used to remove pixels contaminated by clouds or cloud shadows. Due to cloud contamination, some trailcam locations did not have enough HLS data points for constructing satellite-based phenological time series. In these cases, we added pixel values extracted from several Landsat-7 ETM+ images to our analyses. Although the ETM+ product is not radiometrically calibrated to HLS, Mishra et al. (2014) showed that radiances obtained simultaneously from the Landsat-7 ETM+ and Landsat-8 OLI instruments are already closely aligned. Also, we applied the outlier filtering (see Section 3.4) to further reduce discrepancies between Landsat-7 ETM+ and HLS products.

3.2.2. MODIS images

The MODIS NBAR product (MCD43A4, Version 006; Schaaf et al., 2002) provides daily surface reflectance for seven spectral bands at a spatial resolution of 500 m, from which we use only those bands centered at 470 nm (blue), 640 nm (red), and 858 nm (NIR). The MCD43A4 product uses both NASA Aqua (MYD09) and NASA Terra (MOD09) daily reflectance observations within a 16-day period to correct the BRDF effect of the land surface and produces reflectance values as if viewed in nadir orientation. In this work we used only reflectance values indicated as “good” in the product quality assessment image (QA = 0, with full BRDF inversions).

3.3. Vegetation index

For this study, we used the Enhanced Vegetation Index (EVI; Huete et al., 2002) as our indicator of greenness in satellite (HLS and MODIS) pixels. EVI was calculated as:

$$EVI = 2.5 \times \frac{R_{NIR} - R_{red}}{R_{NIR} + 6.0 \times R_{red} - 7.5 \times R_{blue} + 1.0} \quad (3)$$

where R_{blue} , R_{red} and R_{NIR} are the pixel reflectance values (range 0–1) in the blue, red, and NIR bands, respectively, from either HLS, Landsat, or MODIS sources (see Section 3.2.2). EVI is useful for reduction of atmospheric distortion (e.g., from thin cirrus clouds, smoke and haze, etc.) and as an indicator of vegetation photosynthetic vigor that does not saturate in areas of high leaf area index (LAI) like the Normalized Difference Vegetation Index (NDVI).

3.4. Extracting phenological transition dates

A procedure detailed by Richardson et al. (2018a,b) was used to

remove outliers and otherwise smooth the ground-based GCC and MODIS-based EVI time series. Shown here in Fig. 3a, this approach iterates over the time series (the blue and red dots) using a moving window to fit local spline curves (the black curve) and to identify data points as outliers (the red dots) that lie more than two standard deviations above or one standard deviation below the fitted splines. However, we found that this method did not work well for the HLS-based EVI time series, likely because those contained fewer observations than the trailcam- and MODIS-based time-series, making the fitted spline curves more sensitive to localized subsets within the time series. For the HLS-based time series, we iteratively fitted a global logistic function (described below) and removed as outliers those observations occurring more than ± 0.05 EVI units from the fitted curve.

Three methods were used to extract key phenological transition dates from the time series: (1) a four-parameter logistic-curve method (Zhang et al., 2003), (2) a threshold-based method using the fitted spline curves (Richardson et al., 2018a,b), and (3) a piecewise-continuous sine-curve method (Garcia, 2018). We added the sine-curve approach because testing indicated that its fitting resulted in lower RMSE than other approaches (Garcia, 2018). The logistic-curve and sine-curve methods fit the spline-smoothed time series in two separate parts, with DOY 1–200 for the spring season and DOY 200–365 for the autumn season (see Fig. 3b and d), using the equations in Table 1.

Six phenologically significant transition dates (Fig. 3c) were extracted from these fitted curves by finding the local minima, maxima, or inflection points of the fitted curves (Garcia, 2018; Zhang et al., 2003): the start of spring (SOS), spring inflection (SI), start of maturity (SOM), end of maturity (EOM), autumn inflection (AI), and end of autumn (EOA). For the threshold method, these dates were identified when 10% (for SOS and EOA), 50% (for SI and AI), and 90% (for SOM and EOM) of the time series amplitude were reached.

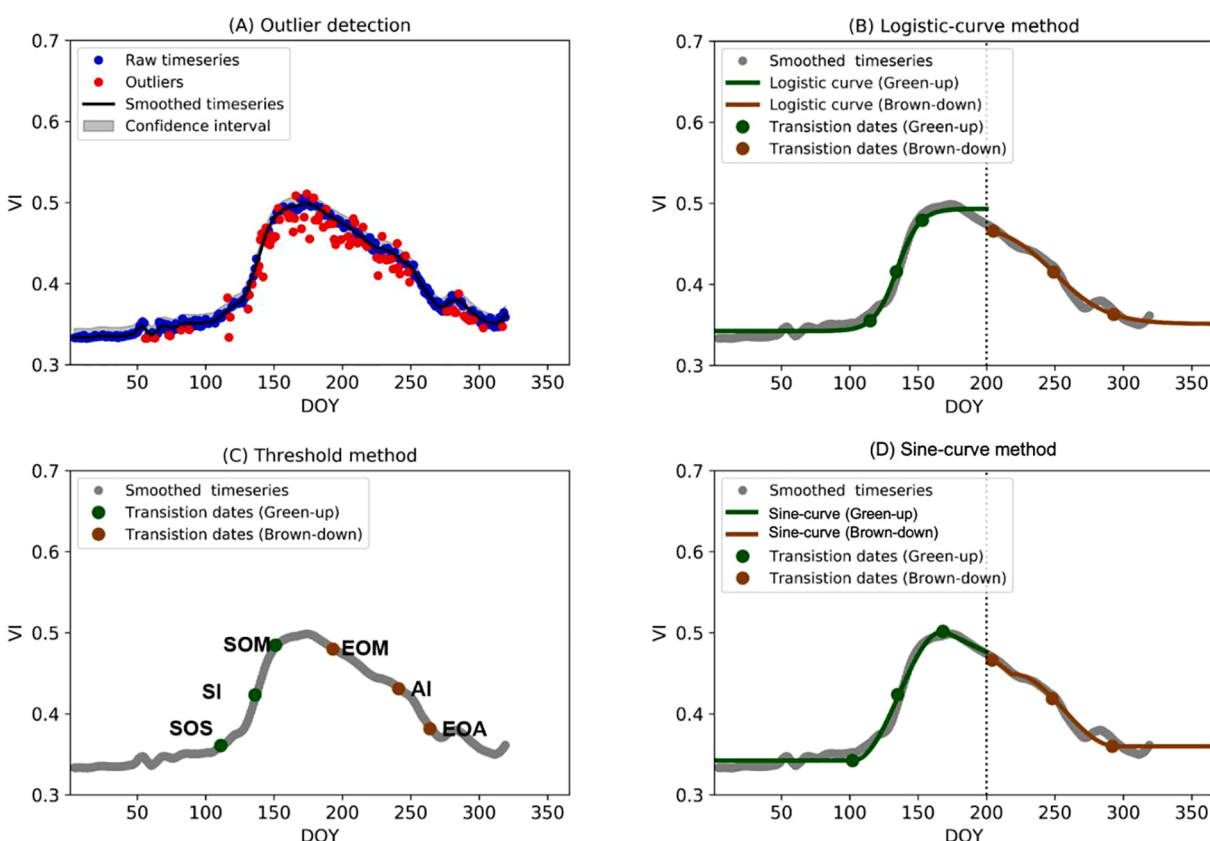


Fig. 3. Outlier detection using fitted spline curves (a) and the three extraction methods used to identify phenological transition dates (b–d) as described in the text. Note that spring (DOY 1–200) and autumn (DOY 200–365) periods are fitted separately using the indicated methods.

Table 1
Logistic-curve and sine-curve methods.

Model	Period	Formula
Logistic-curve	Spring	$VI_{SOS} + \frac{VI_{SOM} - VI_{SOS}}{1 + e^{(DOY - SI)}} \quad 1 \leq DOY \leq 200$
	Autumn	$VI_{EOA} + \frac{VI_{EOM} - VI_{EOA}}{1 + e^{(DOY - AI)}} \quad 200 \leq DOY \leq 365$
Sine-curve	Spring	$\begin{cases} \frac{V_{SOS} + V_{SOM}}{2} + \frac{V_{SOM} - V_{SOS}}{2} \times \sin\left(\left(DOY - \frac{SOM + SOS}{2}\right) \times \frac{\pi}{SOM - SOS}\right) & SOS < DOY < SOM \\ \frac{VI_{200} - VI_{SOM}}{200 - SOM} \times (DOY - SOM) + VI_{SOM} & SOM \leq DOY \leq 200 \end{cases}$
	Autumn	$\begin{cases} \frac{VI_{EOM} - VI_{200}}{EOM - 200} \times (DOY - 200) + VI_{EOM} & 200 \leq DOY \leq EOM \\ \frac{V_{EOA} + V_{EOM}}{2} - \frac{V_{EOM} - V_{EOA}}{2} \times \sin\left(\left(DOY - \frac{EOM + EOA}{2}\right) \times \frac{\pi}{EOA - EOM}\right) & EOM < DOY < EOS \\ VI_{EOA} & EOS \leq DOY \leq 365 \end{cases}$

SOS: start of spring; SI: spring inflection; SOM: start of maturity.

EOA: end of autumn; AI: autumn inflection; EOM: end of maturity.

VI_{DOY}: the VI value on a particular DOY; DOY: Day-Of-Year.

3.5. Statistical analysis

To test the utility of the datasets and their relationships to each other, we compared phenological dates derived by the three extraction methods, differences in phenology between understory vegetation and the overstory canopy, and differences in phenology derived at different spatial scales using satellite-based observations. To evaluate their consistency, we calculated the following statistics for each comparison: the Pearson correlation coefficient (r) between paired samples, the difference in means between the two samples, and Student's paired t -test to indicate those differences in sample means that are significant at $p = 0.05$.

4. Results

4.1. Comparisons of phenological indicators across curve-fitting methods

We use the logistic-curve methods as our “base” result for comparisons with other methods, largely because logistic methods are most common in the literature (Atkinson et al., 2012; Beck et al., 2006). It should be noted that the phenology results from HLS images were not used here since we applied only logistic-curve fitting to that dataset (see Section 3.4). The SOS and EOA dates derived from the three methods align along a 1:1 line, but have substantial offsets when comparing understory, overstory and MODIS phenology (Fig. 4). Moderate to strong correlations ($r = 0.55$ –0.84, with all observations used) were found among the methods. The logistic-curve method had the strongest correlation with the sine-curve method, which was not surprising considering both of these methods use global functions with similar shapes, while the threshold method uses local spline functions to fit the time series. The threshold method produced some extremely early SOS dates (circled in Fig. 4A). In addition, the EOA estimated by the threshold method tended to an asymptote near DOY 300 while the EOA derived from the logistic-curve method increased among sites (Fig. 4C). This illustrates why the correlation between the logistic-curve and threshold methods was weaker than that between the logistic-curve and sine-curve methods.

The t -test results indicated that there were statistically significant differences in phenological transition dates derived by the different curve-fitting and extraction methods. The threshold method yielded a later SOS and earlier EOA than the logistic-curve method, with average differences between these two methods of 4.0 days for SOS and 15.0 days for EOA. The sine-curve method, however, produced an earlier SOS (by 6.7 days) and later EOA (by 8.7 days) than the logistic-curve method. The overall growing season length (SOS to EOA) estimated by

the threshold method was thus 19.0 days longer than that estimated by the logistic-curve method, while the sine-curve estimated growing season to be 14.9 days shorter than that using the logistic-curve.

4.2. Comparison of overstory and understory indicators using trailcam images

The unique perspective of the trailcam image dataset, located just above the ground and often well below the forest canopy, provides an opportunity to distinguish between forest understory and overstory phenological phases in a manner that is typically not available from satellite-based observations. Figs. 5 and 6 compare phenological transition dates (SOS and EOA, respectively) for understory vegetation and overstory canopies as derived from trailcam observations. To avoid unwanted model-related effects, such as a phenological offset between understory and overstory caused by different curve-fitting models, the understory and overstory results from the three methods were assessed separately. In general, weak to moderate correlations ($r = 0.17$ –0.59) were found between understory and overstory canopies for each method and phenological stage. However, the correlations of SOS for the evergreen and mixed forest locations should be taken with some caution due to small sample sizes (evergreen forest: $N = 8$; mixed forest: $N = 7$).

For trailcams in broadleaf deciduous forests, t -tests indicated significantly earlier SOS and later EOA for the understory vegetation compared to the overstory canopy. The magnitude of this phenological difference varied with the fitting method used: the SOS difference between understory and overstory was nearly 6 days by the logistic-curve method but more than 8 days by the other two methods.

For trailcams located in evergreen forests, however, the differences between understory and overstory phenology were less consistent among the various curve-fitting methods. The logistic-curve method suggested that the SOS of the evergreen understory was significantly earlier than that of the overstory, although the other methods suggested the opposite: the SOS of the evergreen understory was later than that of the overstory canopy, though not significantly so. The EOA of the evergreen understory was later than that of the overstory canopy by the sine-curve (statistically significant) and threshold (not statistically significant) methods, while the logistic-curve method showed no differences in understory/overstory EOA phenology.

Finally, for trailcams located in mixed forests, all methods suggested that the understory had an earlier SOS than the overstory, though this difference was statistically significant only for the sine-curve method. For the EOA phenological transition in mixed forests, none of the curve-fitting methods showed significant differences between understory and overstory phenology.

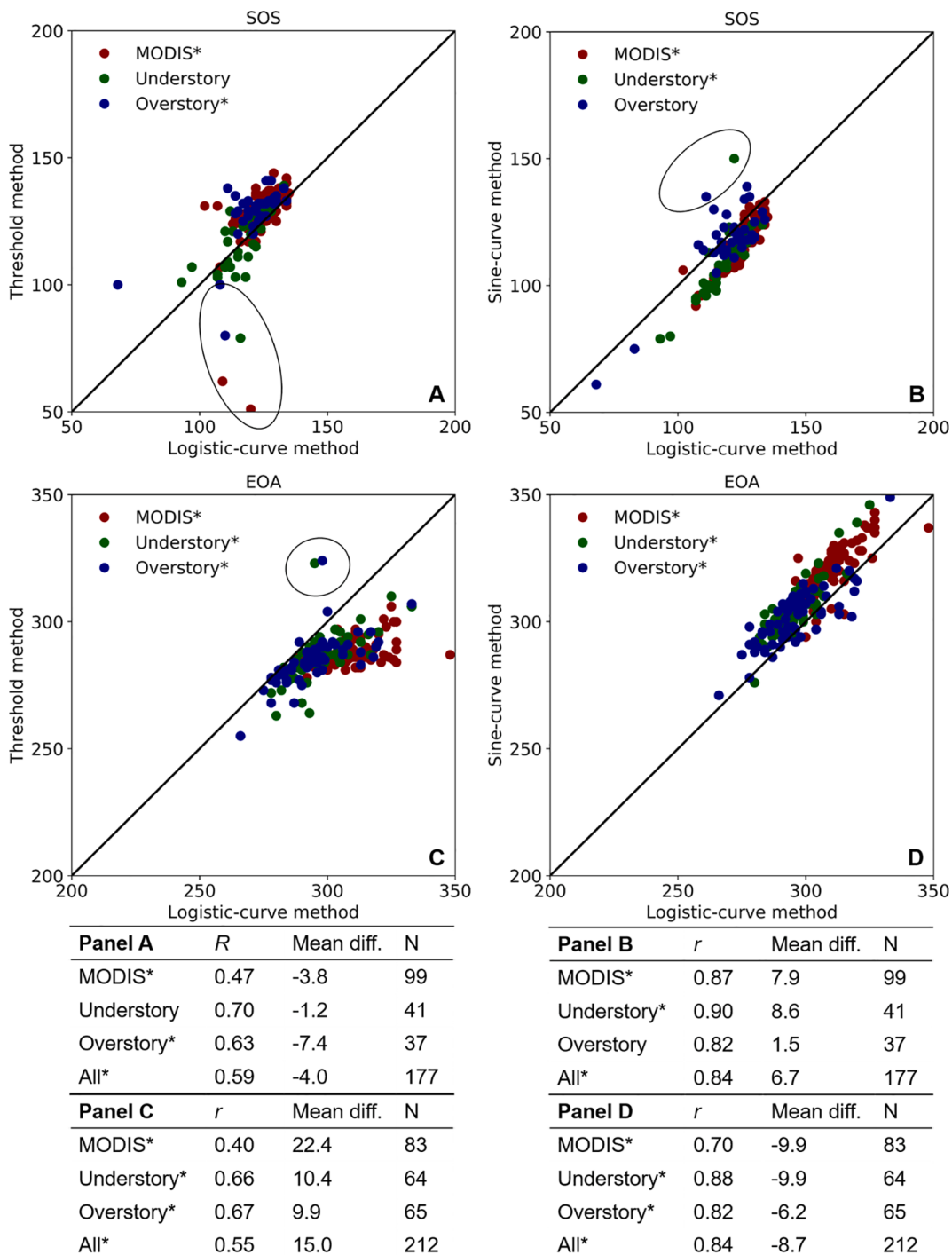


Fig. 4. Comparison of the logistic-curve method with other methods (left column: the threshold method; right column: the sine-curve method). The tables show: (1) Pearson correlation coefficient (r); (2) the mean difference (Mean diff.) in dates between the logistic-curve method and other methods; and (3) the number of cameras (N) in the comparison. Circles in figures: phenological date outliers; see text for discussion. Asterisks indicate statistically significant differences in mean values via Student's t -test at $p = 0.05$. Comparisons here were conducted using only MODIS and trailcam-based estimates.

4.3. Comparison of phenological indicators across observation scales

The general trends of SOS and EOA are comparable between the trailcam observations of understory vegetation and overstory canopy for MODIS retrievals (Fig. 7). The MODIS observations themselves cannot be separated into understory and overstory components, but these comparisons enable interpretation of the contributions of overstory and understory vegetation to surface phenology as sensed by MODIS. To mitigate the scale differences between 500-m MODIS pixels and a

wedge-shaped area approximately 20–50 m across within the trailcam field-of-view (depending on vegetation density), we: (1) calculated the percentage of the dominant land cover within each MODIS pixel using the Wiscland-2.0 land cover map, (2) compared that result with the cover types observed at the trailcam locations, and then (3) excluded pairs of trailcams and corresponding MODIS pixels in which that cover type covered less than 70% of the MODIS pixel. Although this substantially reduced our sample size, all of the remaining MODIS pixels examined here can therefore be considered relatively ‘pure’ pixels and of

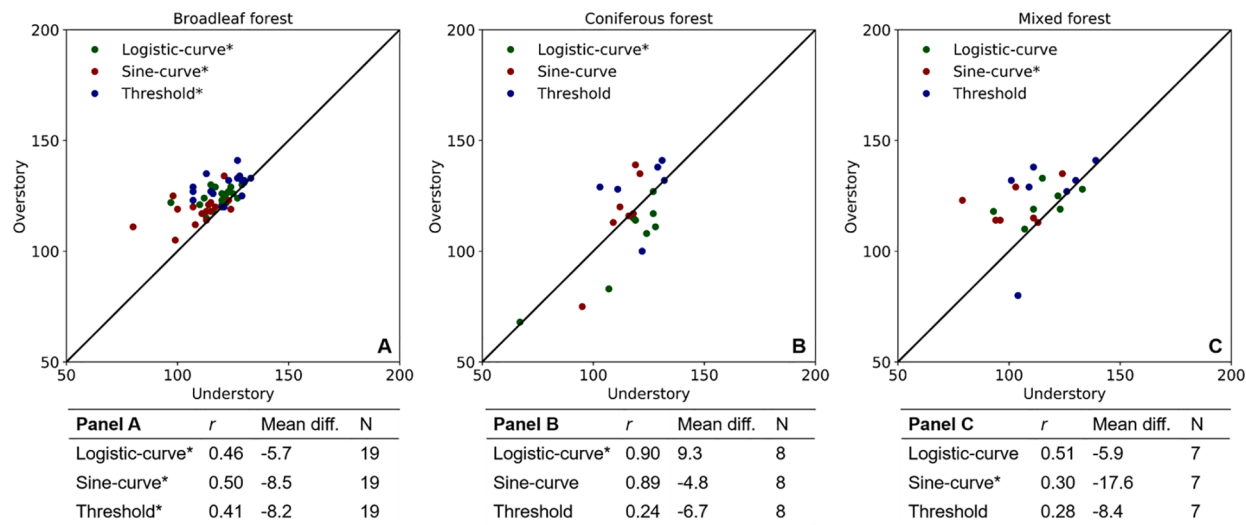


Fig. 5. Comparisons of understory and overstory SOS retrievals using trailcam images. Top row: scatter plots for all curve-fitting methods (*: statistically significant difference in mean values via Student's *t*-test at $p = 0.05$). Bottom row: (1) Pearson correlation coefficients (*r*); (2) the average phenological differences (Mean diff.) between understory and overstory SOS; and (3) sample size of cameras (N).

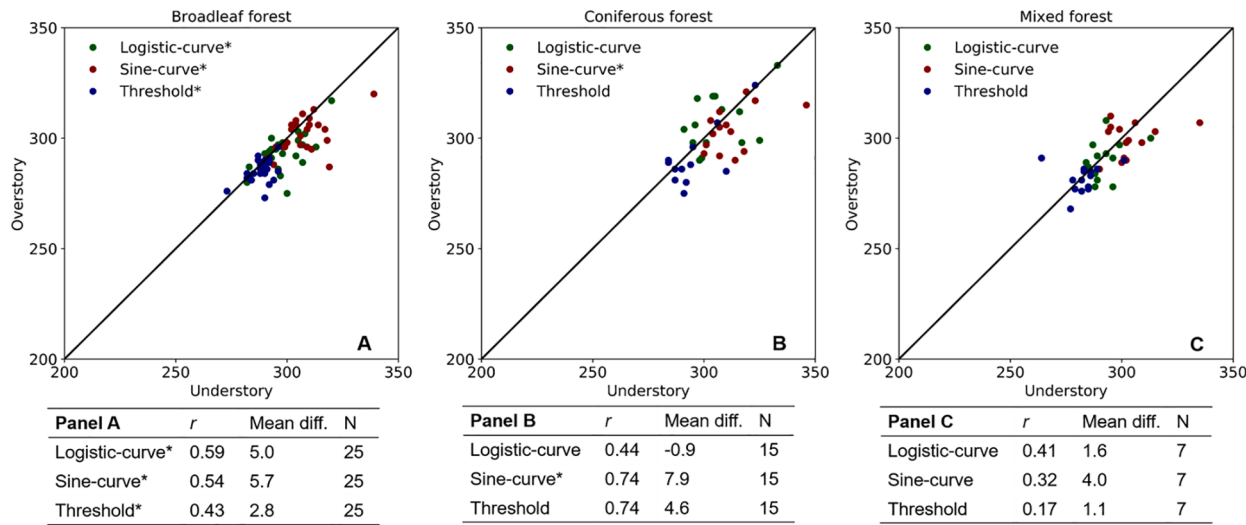


Fig. 6. Comparisons of understory and overstory EOA retrievals using trailcam images. Top row: scatter plots for all curve-fitting methods (*: statistically significant difference in mean values via Student's *t*-test at $p = 0.05$). Bottom row: (1) Pearson correlation coefficients (*r*); (2) the mean phenological differences (Mean diff.) between understory and overstory EOA; and (3) sample size of cameras (N).

a forest type that is consistent with the corresponding trailcam observations on the ground.

There was a moderate correspondence between MODIS and trailcam phenology at SOS and EOA, with correlations found in the range $r = 0.25\text{--}0.57$. For SOS, Student's *t*-test indicated that curve fitting methods applied to MODIS observations yield understory green-up dates significantly later than observed in trailcam time series. This is highly relevant to ecological interpretations of satellite phenology because understory green-up is a significant indicator of the onset of biological activity, as root processes commence prior to budburst and wildlife are dependent on high-nutrition early-season undergrowth for sustenance (Bischof et al., 2012). The average SOS difference between trailcam-based understory and MODIS retrievals ranged from 6.6 to 11.4 days, depending on the curve-fitting and phenological extraction methods used.

For EOA, Student's *t*-test showed that the MODIS-based retrievals were generally later than both understory and overstory senescence in trailcam-based time series, with differences ranging from 8.7 to 14.8 days. Overall, in comparison to trail camera observations, MODIS

appears to observe the green-up of the overstory canopy most accurately, showing statistically insignificant differences from trailcam observations only for overstory SOS dates, but exhibits a lag ranging from 2 days to 2 weeks for understory SOS and both overstory and understory EOA forest phenology regardless of the curve-fitting and phenological extraction methods used.

SOS and EOA estimates for the trailcam observations of understory vegetation and overstory canopy correlated weakly with HLS retrievals, and only where sample sizes were sufficient (Fig. 8). Compared to MODIS-derived results, the correspondence between HLS- and trailcam-based phenology was poorer, with correlations found in the range $r = 0.22\text{--}0.33$. Student's *t*-test showed that the SOS of understory and overstory for coniferous forest was later than that of HLS.

5. Discussion

Variability in the curve-fitting and methods used to determine key phenological transition dates from satellite-based datasets can strongly

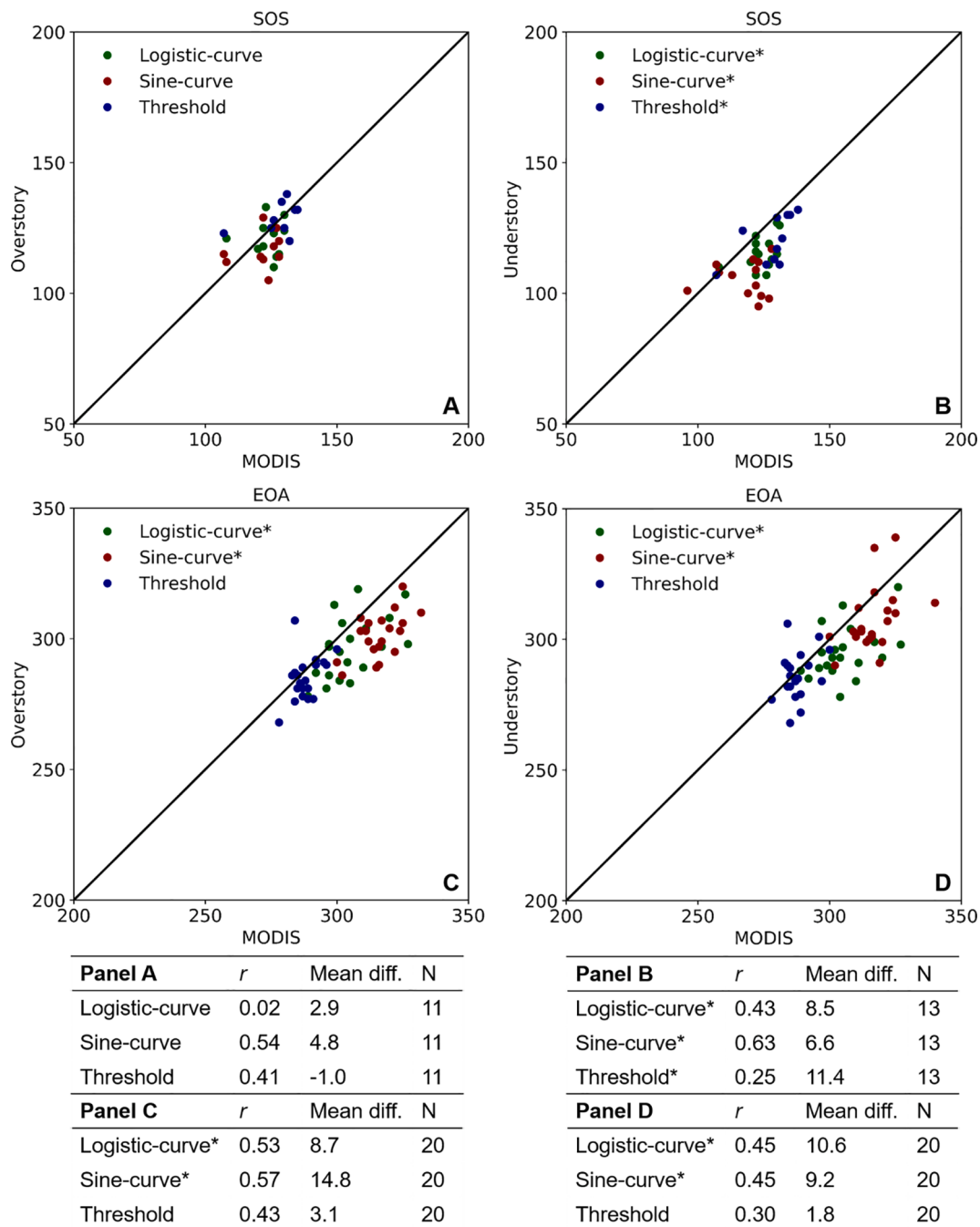


Fig. 7. Comparison of MODIS and trailcam-based SOS and EOA retrievals. Asterisk indicates statistically significant difference in mean values via Student's *t*-test at $p = 0.05$; N: sample size of cameras; *r*: Pearson correlation coefficient; Mean diff.: the mean phenological differences between MODIS and trailcam-based phenology dates.

influence our characterization of the phenological cycle. In this study, comparisons with in-situ trailcam observations have helped us quantify uncertainties in growing-season phenology resulting from different curve-fitting methods that range from -8.9 to +14.6 days. Though this is a smaller range than found in previous studies (de Beurs and Henebry, 2010; Schwartz and Hanes, 2010; White et al., 2014), large uncertainties in satellite-derived phenology may have significant ramifications in the modelling of vegetation processes, quantifying nutrient cycles, and linking wildlife patterns to vegetation dynamics. Quantification of these uncertainties is important given that large areas of Earth lack in-situ data necessary to facilitate such comparisons. To take an example from carbon accounting in climate models, Jeong et al. (2012) showed that greater uncertainty in observed leaf onset dates led to greater

variability in the estimated date when the ecosystem switches from a carbon source to a carbon sink. At smaller scales, as in wildlife ecology, such uncertainty can affect predictions of the availability of food resources (Bater et al., 2011), leading to large variability in population modeling outcomes. However, there remains a general lack of consensus on a preferred approach to satellite-based phenological analysis that could effectively reduce such uncertainties at all scales of application (Atkinson et al., 2012; de Beurs and Henebry, 2010; White et al., 2014, 2009).

When situated appropriately, trailcams offer a unique perspective for observing differences between understory and overstory phenology (Kobayashi et al., 2016; Liang et al., 2012). This is important when interpreting satellite-based phenology – i.e., land surface phenology –

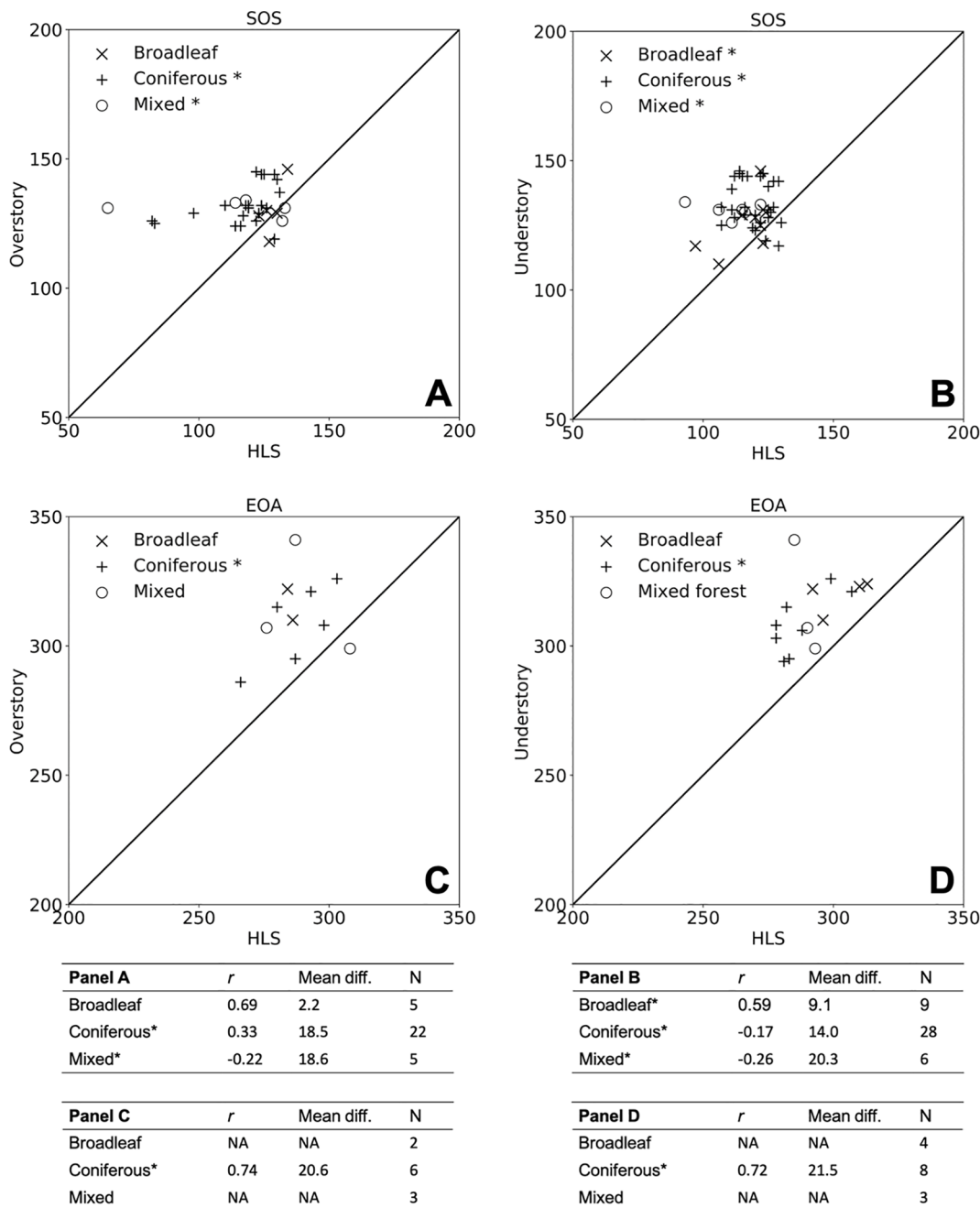


Fig. 8. Comparison of HLS and trailcam-based SOS and EOA retrievals. Asterisk indicates statistically significant difference in mean values via Student's *t*-test at $p = 0.05$; N: sample size of cameras; r: Pearson correlation coefficient; Mean diff.: the mean phenological differences between HLS and trailcam-based phenology dates. Student's *t*-test was only applied to the coniferous SOS due to sample size.

which incorporates greenness from only those components of the vegetation are exposed to the sensor. A phenological offset (earlier SOS and/or later EOA) between understory and overstory vegetation has been reported in previous studies (Augspurger and Bartlett, 2003; Mahall and Bormann, 1978; Richardson and O'Keefe, 2009; Sparling, 1967; Uemura, 1994). In deciduous forests, understory vegetation may often green up earlier and senesce later than the overstory canopy to make greatest use of seasonal patterns in light availability (Kato and Komiyama, 2002; Richardson and O'Keefe, 2009). From the satellite perspective, however, phenological analyses can easily mistake early understory green-up for leaf development in the forest overstory or miss low-density understory vegetation entirely. In the late spring and early autumn, much of the photosynthetically active radiation (PAR) reaching the ground must pass through the overstory canopy, so the transmitted

PAR becomes more restricted with canopy closure. Through a strategy of "phenological escape" (Richardson and O'Keefe, 2009), shade-intolerant understory plants can take advantage of the high PAR before overstory canopy closure in the spring and after overstory senescence in the autumn. In our study, this understory phenological escape was most apparent in the broadleaf deciduous forest for both SOS and EOA, and in the mixed forest for SOS (see Figs. 5 and 6). The mean difference between understory and overstory SOS (~8 days) was comparable to that reported in previous studies (Richardson and O'Keefe, 2009).

The extraction of evergreen needleleaf forest phenology from both trailcam and satellite sources remains a greater challenge, also as noted in previous studies (Bolton et al., 2020; Delbart et al., 2005; Jin and Eklundh, 2014; White et al., 2014). Seasonal VI variation ((max-min)/

max) was substantially smaller in the evergreen ($22.22\% = (0.45-0.35)/0.45$) than in the broadleaf deciduous forest ($41.81\% = (0.55-0.32)/0.55$). Bolton et al. (2020) recently derived a 30-m resolution land surface phenology product from the HLS images for Northern America. When validating the HLS-derived phenology with field PhenoCam-derived phenology, they found that 33 of 96 site-years did not have VI amplitudes greater than the prescribed minimum required by the algorithm to determine a phenological cycle. In addition, the presence of snow on coniferous trees around SOS and EOA greatly affected VI retrievals around those dates (Jin and Eklundh, 2014), introducing large uncertainties in the estimation of evergreen seasonal phenology. Finally, many evergreen species may extend their needleleaf canopy all the way to the ground and may not support the consistent growth of understory vegetation. Overall, we found no consistent phenological differences between the evergreen forest overstory canopy and understory (Fig. 5), likely due to a relatively deficient and unvarying understory light environment when compared to deciduous and mixed deciduous forest locations.

In this study, we investigated the phenological patterns of understory plants without regard to the many different species that exhibit varying adaptation strategies in the limited understory light environment (Mahall and Bormann, 1978; Richardson and O'Keefe, 2009). Mahall and Bormann (1978) found that species that green up early such as *Erythronium americanum* (yellow trout lily) and *Claytonia virginica* (Virginia springbeauty), both present in Wisconsin deciduous broadleaf forests and known as vernal photosynthetics, tended to occur in locations with high early-season PAR, while other species such as *Uvularia sessilifolia* (wild oats) and *Clintonia borealis* (blue-bead lily), also both present in Wisconsin forests, were more shade-tolerant and adapted to low PAR, remaining green in the understory environment well into the summer. As a result, vernal photosynthetic species may emerge soon after snowmelt but then abruptly senesce when the overstory canopy closes, while summer green species exhibit more gradual leaf expansion before overstory canopy closure and tend to endure through the summer shade period. Future research may focus on obtaining in situ observations of phenological dynamics in different understory species and linking them to the phenological patterns observed from trailcams.

It should be noted that numerous factors in addition to PAR such as air temperature and humidity (microclimatology), soil quality and nutrient availability, and local-scale hydrology are important drivers of understory phenology (Dittman et al., 2007; Keenan and Richardson, 2015; Laskin et al., 2019; Liang et al., 2012; Piao et al., 2019; Yu et al., 2016). Liang et al. (2012) found that understory vegetation was more sensitive than the overstory canopy to day-to-day changes in humidity during relatively dry growing seasons. Laskin et al. (2019) showed that the daily understory air temperature measured at ~1 m above the ground, the approximate height of the SW trailcams, could predict understory phenology well. Some trailcam models record the temperature along with the time on their digital photographs, which could provide an invaluable additional source of data in future studies.

Although HLS offers detailed spatial resolution (~30 m) and good temporal resolution (~5 days) for satellite observations, due to clouds there were still few pixels in 2017 (20–30) available for fitting phenological curves. This data scarcity added uncertainty to the SOS and EOA dates estimated from HLS images in this study and may explain in part why HLS-based phenology correlated poorly with that derived from trailcams. Recent studies have shown that Sentinel-2 has high radiometric and geometric consistency with other satellite data sources such as MODIS (Claverie et al., 2018) and Landsat (Claverie et al., 2018; Guzinski and Nieto, 2019; Pahlevan et al., 2019; Zhang et al., 2018). There is thus great potential for fusing Sentinel-2 observations with other satellite sources to fill gaps in, and improve the density of, growing-season phenological time series (Claverie et al., 2018; Gao et al., 2006; Vrieling et al., 2018; Walker et al., 2012; Wang et al., 2017, 2016). Additional high-resolution data sources, such as daily 3-m Planet imagery with four spectral bands (from which we can calculate EVI),

may enable better linkages between satellite imagery and trailcam photos at more appropriate spatial scales. For instance, Cheng et al. (2020) applied Plant imagery to extract phenology in semi-arid environment. They found that the phenology map derived from fine-scale (3-m) Plant imagery had fewer artifacts than that from coarse-scale (10-m) Sentinel imagery. Moreover, the phenology of individual trees could be differentiated from grassland surroundings by Planet imagery due to its high spatial resolution. However, challenges of applying Planet images at broad scales still remains due to its radiometric calibration (Houborg and McCabe, 2018; Leach et al., 2019; Wegmueller et al., in review). Recent work by Houborg and McCabe (2018) and Sadeh et al. (2021) indicated that 3 m Planet images could be radiometrically integrated with other coarse-scale satellite images (e.g., 10 m Sentinel-2, 30 m Landsat and 500 m MODIS) with a better radiometric quality.

The correlations between trailcam- and MODIS-derived phenology presented here are somewhat weaker than those for phenocam comparisons with MODIS reported in previous studies (Fisher and Mustard, 2007; Hufkens et al., 2012; Liang et al., 2014; Richardson et al., 2018a, b) but remain comparable to previous comparisons using sub-canopy digital cameras (St. Peter et al., 2018). This can be attributed to differences in various settings and fields-of-view between the trailcams and the dedicated phenocams that are used in national and international networks. For phenocam studies, the cameras are situated above the forest canopy expressly to characterize phenology on scales of 10–100 m. The phenocam FOV is therefore comparable with single-pixel areal coverage in satellite images (Fisher and Mustard, 2007; Richardson et al., 2018a,b). All of our trailcams were located beneath the forest overstory, and the area observed by our cameras was much smaller than a MODIS pixel, typically with representative spatial scales less than 20 m depending on the density of understory vegetation. Even though we characterized vegetation types within the trailcam images and excluded strongly mixed MODIS pixels from this analysis, scale-related issues remain prevalent in such comparisons: even within relatively pure MODIS pixels, with at least 70% of the pixel classified as the same cover type that was identified in the corresponding trailcam location, there remains the issue of local phenological variability at finer scales (Fisher and Mustard, 2007). In a recent study by Zhang et al. (2017), the standard deviation of the SOS derived from 30-m resolution Landsat-8 imagery within a heterogenous VIIRS (Visible Infrared Imaging Radiometer Suite) pixel could be 40 days. This is especially true of understory vegetation, which is not characterized in existing land cover classifications. Several potential approaches to mitigating these disparities have been proposed, such as image fusion using coarse-resolution MODIS images and high-resolution images, as from Landsat or Sentinel-2, to adjust and disaggregate the coarse dataset for phenological analysis at fine scales (Gao et al., 2006; Hilker et al., 2009; Roy et al., 2008; Walker et al., 2012; Zhang et al., 2017). Another potential solution involves aggregation of in-situ phenology observed at a collection of nearby field sites to larger scales, such as the area of a MODIS pixel (Bater et al., 2011; Huang et al., 2010; Liang et al., 2011; Liu et al., 2015; Melaas et al., 2016a; Vartanian et al., 2014). Dense trailcam networks represent an alternative methodology to verify satellite-derived metrics of phenology where phenocams or other observations are absent, and to assess the ecological interpretations about ground conditions that can only be inferred (not observed) from satellite data. Because trailcams are usually deployed for reasons other than vegetation monitoring, users must remain mindful of multi-use considerations such as placement, viewshed, and camera movement, all of which reduced the number of cameras available from the SW network for our analyses.

For broadleaf deciduous forests, the land surface SOS derived from MODIS is likely earlier than actual overstory SOS because the MODIS-observed greenness is partially contributed by the understory vegetation (Ahl et al., 2006). In this study, the dominant land cover types in the relatively pure MODIS pixels (see Figs. 7 and 8) were evergreen needleleaf forests. Greenness signals from any understory vegetation in such locations were mostly obscured by the forest canopy because the nadir-

viewing MODIS sees the overstory canopy almost exclusively, meaning that the derived MODIS phenology is due almost entirely to the overstory dynamics, in contrast to that observed in deciduous and mixed forests. Observing understory phenological patterns from space remains challenging due to obstruction by the forest overstory canopy, but the magnitude of this challenge changes with forest type, which then contributes to challenges in the consistent inference of overstory phenology and associated ecological processes from the satellite perspective. This has long been known, but it is worth re-emphasizing: our data confirm that satellite-based estimations of SOS and EOS at locations that include both deciduous and evergreen vegetation are not comparable, and the data must be stratified by land cover type in analyses.

Trailcams may be invaluable in efforts to map understory phenology, an important need for a variety of ecological applications (Prevéy et al., 2020). Other data sources, such as synthetic aperture radar and LiDAR, offer opportunities to identify the presence and density of understory vegetation, if not also its phenology (Salas, 2020), as a basis for data stratification and to help identify the sources of phenological variation observed in satellite imagery. Different data types, such as satellite images and camera networks, could be fused within hybrid or integrated models that draw from both sources to produce better-informed maps of phenology (Pacifici et al., 2017), although accounting for spatial and temporal misalignment between data streams could require advanced and computationally intensive statistical approaches (Banerjee and Gelfand, 2002). Alternatively, gridded understory phenology products could be generated from large and dense networks of trail cameras or other ancillary data streams alone using geostatistical approaches, or such networks could be used to develop correction factors for existing MODIS and HLS products (Sirén et al., 2018). The emergence of observation programs like SW and other broad-scale camera deployments (Steenweg et al., 2017) makes such approaches increasingly promising. As well, additional data can be integrated: Laskin et al. (2016, 2019) used MODIS-derived land surface temperature (LST) and LiDAR-derived forest structure to model daily air temperature in the understory layer, from which they were able to derive realistic patterns of understory phenology. However, a large number of temperature observations from ground-based thermal sensors was still required to calibrate their model, and comparable data at the trailcam-scale were not yet available for our study here. Issues of phenological interpretation due to scale differences persist and remain the subject of ongoing work.

6. Conclusion

In this study we demonstrated the application of a digital trailcam network, part of the Snapshot Wisconsin citizen science effort, to characterize forest understory and overstory phenology. Retrievals from different data sources and curve-fitting methods were compared. Trailcam photos enabled discrimination of phenological differences between understory vegetation and the forest overstory canopy, owing to a sub-canopy oblique view that captures multiple elements of forest structure. In the broadleaf deciduous and mixed forest locations, understory vegetation tended to green up approximately one week earlier than the overstory canopy, a difference that may reflect the abundance of understory species adapted to early-season light conditions. Satellite-derived phenology from MODIS showed moderate correlations with trailcam-based SOS and EOA dates, with the best agreement occurring for deciduous overstories. Offsets in timing between trailcam- and satellite-based estimates of phenological transition dates are consistent with the inherent inability of nadir-viewing satellite observations to distinguish between understory and overstory vegetation over large areas and especially with mixed pixels. The issue of scale mismatch between ground- and satellite-based observations remained prevalent in results based on MODIS-derived phenology. However, in the absence of extensive ground networks for validation of satellite phenology, data from trailcams represent an important corroborating source for interpretations from satellite imagery.

Despite the limitations of ground-based trailcams for characterizing phenology at high density over large scales, we think that emerging trailcam networks have great potential to inform and enhance phenological studies at local scales. Although trailcams are typically deployed for purposes other than phenological observations, programming those trailcams to record additional images at consistent times on a daily basis can provide invaluable information for phenological analyses at locations of great interest. Compared with other ground-based sensors, such as phenocams or flux towers, trailcams are cheaper, easier to install, and thus tend to have a higher spatial observation density. Potentially many more trailcams can be deployed at advantageous locations in ecosystems to address multiple lines of research using fewer resources than phenocams require. Trailcams also have the added benefit of providing direct information on understory phenology. The multiple uses of trailcam data can significantly enhance the ability to diagnose structurally variable forest phenology and to interpret satellite-based remote sensing observations.

CRediT authorship contribution statement

Nanfeng Liu: Conceptualization, Methodology, Software, Validation, Formal analysis, Writing - original draft, Writing - review & editing. **Matthew Garcia:** Conceptualization, Methodology, Software, Validation, Formal analysis, Writing - original draft, Writing - review & editing. **Aditya Singh:** Conceptualization, Methodology, Software, Writing - review & editing. **John D.J. Clare:** Resources. **Jennifer L. Stenglein:** Resources. **Benjamin Zuckerberg:** Writing - review & editing. **Eric L. Kruger:** Writing - review & editing. **Philip A. Townsend:** Conceptualization, Methodology, Writing - original draft, Writing - review & editing.

Declaration of Competing Interest

The authors declare that they have no known competing financial interests or personal relationships that could have appeared to influence the work reported in this paper.

Acknowledgments

This research was funded by NASA Ecological Forecasting grant NNX14AC36G, with additional support partially provided by the USFWS Pittman-Robertson Wildlife Restoration Program. MG received support from the USDA Forest Service and Natural Resources Canada. JC received support from NASA Earth and Space Science Fellowship award NNX16A061H. The authors also acknowledge considerable logistic support from the Wisconsin Department of Natural Resources (WDNR). Thanks to Young Lee who assisted with the Python programming, and to Dewi Atikah Radin Umar, Ben Townsend, Sawyer Boldt, Zhixing Xu, and Lena Carlson who assisted with photo interpretation. Thank you to the thousands of Snapshot Wisconsin volunteers who were essential to data collection and processing, especially the trail camera hosts.

Appendix A. Supplementary material

Supplementary data to this article can be found online at <https://doi.org/10.1016/j.jag.2020.102291>.

References

- Ahl, D.E., Gower, S.T., Burrows, S.N., Shabanov, N.V., Myneni, R.B., Knyazikhin, Y., 2006. Monitoring spring canopy phenology of a deciduous broadleaf forest using MODIS. *Remote Sens. Environ.* 104, 88–95. <https://doi.org/10.1016/j.rse.2006.05.003>.
- Atkinson, P.M., Jegannathan, C., Dash, J., Atzberger, C., 2012. Inter-comparison of four models for smoothing satellite sensor time-series data to estimate vegetation phenology. *Remote Sens. Environ.* 123, 400–417. <https://doi.org/10.1016/j.rse.2012.04.001>.

- Augspurger, C.K., Bartlett, E.A., 2003. Differences in leaf phenology between juvenile and adult trees in a temperate deciduous forest. *Tree Physiol.* 23, 517–525. <https://doi.org/10.1093/treephys/23.8.517>.
- Ault, T.R., Schwartz, M.D., Zurita-Milla, R., Weltzin, J.F., Betancourt, J.L., 2015. Trends and natural variability of spring onset in the coterminous United States as evaluated by a new gridded dataset of spring indices. *J. Clim.* 28, 8363–8378. <https://doi.org/10.1175/JCLI-D-14-00736.1>.
- Badeck, F.-W., Bondeau, A., Bottcher, K., Doktor, D., Lucht, W., Schaber, J., Sitch, S., 2004. Responses of spring phenology to climate change. *New Phytol.* 162, 295–309. <https://doi.org/10.1111/j.1469-8137.2004.01059.x>.
- Banerjee, S., Gelfand, A.E., 2002. Prediction, Interpolation and Regression for Spatially Misaligned Data. *Sankhyā Indian J. Stat. Ser. A* 64, 227–245.
- Bater, C.W., Coops, N.C., Wulder, M.A., Hilker, T., Nielsen, S.E., McDermid, G., Stenhouse, G.B., 2011. Using digital time-lapse cameras to monitor species-specific understory and overstorey phenology in support of wildlife habitat assessment. *Environ. Monit. Assess.* 180, 1–13. <https://doi.org/10.1007/s10661-010-1768-x>.
- Beck, P.S.A., Atzberger, C., Högda, K.A., Johansen, B., Skidmore, A.K., 2006. Improved monitoring of vegetation dynamics at very high latitudes: A new method using MODIS NDVI. *Remote Sens. Environ.* 100, 321–334. <https://doi.org/10.1016/j.rse.2005.10.021>.
- Bischof, R., Loe, L.E., Meisingset, E.L., Zimmermann, B., Van Moorert, B., Mysterud, A., 2012. A migratory northern ungulate in the pursuit of spring: jumping or surfing the green wave? *Am. Nat.* 180, 407–424. <https://doi.org/10.1086/667590>.
- Bolton, D.K., Gray, J.M., Melaas, E.K., Moon, M., Eklundh, L., Friedl, M.A., 2020. Continental-scale land surface phenology from harmonized Landsat 8 and Sentinel-2 imagery. *Remote Sens. Environ.* 240, 111685. <https://doi.org/10.1016/j.rse.2020.111685>.
- Brown, T.B., Hultine, K.R., Steltzer, H., Denny, E.G., Denslow, M.W., Granados, J., Henderson, S., Moore, D., Nagai, S., SanClementes, M., Sánchez-Azofeifa, A., Sonnentag, O., Tazik, D., Richardson, A.D., 2016. Using phenocams to monitor our changing Earth: Toward a global phenocam network. *Front. Ecol. Environ.* 14, 84–93. <https://doi.org/10.1002/fee.1222>.
- Chen, J., Jönsson, P., Tamura, M., Gu, Z., Matsushita, B., Eklundh, L., 2004. A simple method for reconstructing a high-quality NDVI time-series data set based on the Savitzky-Golay filter. *Remote Sens. Environ.* 91, 332–344. <https://doi.org/10.1016/j.rse.2004.03.014>.
- Cheng, Y., Vrieling, A., Fava, F., Meroni, M., Marshall, M., Gachoki, S., 2020. Phenology of short vegetation cycles in a Kenyan rangeland from PlanetScope and Sentinel-2. *Remote Sens. Environ.* 248, 112004. <https://doi.org/10.1016/j.rse.2020.112004>.
- Chmielewski, F.M., Rötter, T., 2001. Response of tree phenology to climate change across Europe. *Agric. For. Meteorol.* 108, 101–112. [https://doi.org/10.1016/S0168-1923\(01\)00233-7](https://doi.org/10.1016/S0168-1923(01)00233-7).
- Clare, J.D.J., Townsend, P.A., Anhalt-Depies, C., Locke, C., Stenglein, J.L., Frett, S., Martin, K.J., Singh, A., Van Deelen, T.R., Zuckerberg, B., 2019. Making inference with messy (citizen science) data: when are data accurate enough and how can they be improved? *Ecol. Appl.* 29, e01849. <https://doi.org/10.1002/eaap.1849>.
- Claverie, M., Ju, J., Masek, J.G., Dungan, J.L., Vermote, E.F., Roger, J.-C., Skakun, S.V., Justice, C., 2018. The Harmonized Landsat and Sentinel-2 surface reflectance data set. *Remote Sens. Environ.* 219, 145–161. <https://doi.org/10.1016/j.rse.2018.09.002>.
- Cleland, E., Chuique, I., Menzel, A., Mooney, H., Schwartz, M., 2007. Shifting plant phenology in response to global change. *Trends Ecol. Evol.* 22, 357–365. <https://doi.org/10.1016/j.tree.2007.04.003>.
- Desai, A.R., 2010. Climatic and phenological controls on coherent regional interannual variability of carbon dioxide flux in a heterogeneous landscape. *J. Geophys. Res.* 115, G00J02. <https://doi.org/10.1029/2010JG001423>.
- de Beurs, K.M., Henebry, G.M., 2010. Spatio-temporal statistical methods for modelling land surface phenology, in: *Phenological Research*. Springer Netherlands, Dordrecht, pp. 177–208. https://doi.org/10.1007/978-90-481-3335-2_9.
- Delbart, N., Kergoat, L., Le Toan, T., Lhermitte, J., Picard, G., 2005. Determination of phenological dates in boreal regions using normalized difference water index. *Remote Sens. Environ.* 97, 26–38. <https://doi.org/10.1016/j.rse.2005.03.011>.
- Dittman, J.A., Driscoll, C.T., Groffman, P.M., Fahey, T.J., 2007. Dynamics of nitrogen and dissolved organic carbon at the Hubbard Brook experimental forest. *Ecology* 88, 1153–1166. <https://doi.org/10.1890/06-0834>.
- Dong, J., Xiao, X., Kou, W., Qin, Y., Zhang, G., Li, L., Jin, C., Zhou, Y., Wang, J., Biradar, C., Liu, J., Moore, B., 2015. Tracking the dynamics of paddy rice planting area in 1986–2010 through time series Landsat images and phenology-based algorithms. *Remote Sens. Environ.* 160, 99–113. <https://doi.org/10.1016/j.rse.2015.01.004>.
- Eklundh, L., Jönsson, P., 2016. TIMESAT for processing time-series data from satellite sensors for land surface monitoring. In: Ban, Y. (Ed.), *Multitemporal Remote Sensing. Remote Sensing and Digital Image Processing*. Springer, Cham, pp. 177–194. https://doi.org/10.1007/978-3-319-47037-5_9.
- Elmendorf, S.C., Jones, K.D., Cook, B.I., Diez, J.M., Enquist, C.A.F., Hufft, R.A., Jones, M.O., Mazer, S.J., Miller-Rushing, A.J., Moore, D.J.P., Schwartz, M.D., Weltzin, J.F., 2016. The plant phenology monitoring design for The National Ecological Observatory Network. *Ecosphere* 7, e01303. <https://doi.org/10.1002/ecs2.1303>.
- Filippa, G., Cremonese, E., Migliavacca, M., Galvagno, M., Forkel, M., Wingate, L., Tomelleri, E., Morra di Cellia, U., Richardson, A.D., 2016. Phenopix: A R package for image-based vegetation phenology. *Agric. For. Meteorol.* 220, 141–150. <https://doi.org/10.1016/j.agrformet.2016.01.006>.
- Fisher, J., Mustard, J., Vadéboncoeur, M., 2006. Green leaf phenology at Landsat resolution: Scaling from the field to the satellite. *Remote Sens. Environ.* 100, 265–279. <https://doi.org/10.1016/j.rse.2005.10.022>.
- Fisher, J.I., Mustard, J.F., 2007. Cross-scalar satellite phenology from ground, Landsat, and MODIS data. *Remote Sens. Environ.* 109, 261–273. <https://doi.org/10.1016/j.rse.2007.01.004>.
- Ganguly, S., Friedl, M.A., Tan, B., Zhang, X., Verma, M., 2010. Land surface phenology from MODIS: Characterization of the Collection 5 global land cover dynamics product. *Remote Sens. Environ.* 114, 1805–1816. <https://doi.org/10.1016/j.rse.2010.04.005>.
- Gao, F., Masek, J., Schwaller, M., Hall, F., 2006. On the blending of the Landsat and MODIS surface reflectance: predicting daily Landsat surface reflectance. *IEEE Trans. Geosci. Remote Sens.* 44, 2207–2218. <https://doi.org/10.1109/TGRS.2006.872081>.
- Garcia, M., Townsend, P.A., 2016. Recent climatological trends and potential influences on forest phenology around western Lake Superior USA. *J. Geophys. Res. Atmos.* 121, 13364–13391. <https://doi.org/10.1002/2016JD025190>.
- Garcia, M., 2018. Climatology and Forest Phenology During 1984–2013 Around Western Lake Superior, USA. University of Wisconsin-Madison.
- Guzinski, R., Nieto, H., 2019. Evaluating the feasibility of using Sentinel-2 and Sentinel-3 satellites for high-resolution evapotranspiration estimations. *Remote Sens. Environ.* 221, 157–172. <https://doi.org/10.1016/j.rse.2018.11.019>.
- Haggerty, B.P., Mazer, S.J., 2008. *The Phenology Handbook: A guide to phenological monitoring for students, teachers, families, and nature enthusiasts*. Santa Barbara, California.
- Hilker, T., Wulder, M.A., Coops, N.C., Linke, J., McDermid, G., Masek, J.G., Gao, F., White, J.C., 2009. A new data fusion model for high spatial- and temporal-resolution mapping of forest disturbance based on Landsat and MODIS. *Remote Sens. Environ.* 113, 1613–1627. <https://doi.org/10.1016/j.rse.2009.03.007>.
- Houborg, R., McCabe, M.F., 2018. A Cubesat enabled Spatio-Temporal Enhancement Method (CESTEM) utilizing Planet, Landsat and MODIS data. *Remote Sens. Environ.* 209, 211–226. <https://doi.org/10.1016/j.rse.2018.02.067>.
- Huang, S., Potter, C., Crabtree, R.L., Hager, S., Gross, P., 2010. Fusing optical and radar data to estimate sagebrush, herbaceous, and bare ground cover in Yellowstone. *Remote Sens. Environ.* 114, 251–264. <https://doi.org/10.1016/j.rse.2009.09.013>.
- Huete, A., Didan, K., Miura, T., Rodriguez, E.P., Gao, X., Ferreira, L.G., 2002. Overview of the radiometric and biophysical performance of the MODIS vegetation indices. *Remote Sens. Environ.* 83, 195–213. [https://doi.org/10.1016/S0034-4257\(02\)00096-2](https://doi.org/10.1016/S0034-4257(02)00096-2).
- Hufkens, K., Basler, D., Milliman, T., Melaas, E.K., Richardson, A.D., 2018. An integrated phenology modelling framework in R. *Methods Ecol. Evol.* 9, 1276–1285. <https://doi.org/10.1111/2041-210X.12970>.
- Hufkens, K., Friedl, M., Sonnentag, O., Braswell, B.H., Milliman, T., Richardson, A.D., 2012. Linking near-surface and satellite remote sensing measurements of deciduous broadleaf forest phenology. *Remote Sens. Environ.* 117, 307–321. <https://doi.org/10.1016/j.rse.2011.10.006>.
- Jeong, S.-J., Ho, C.-H., Gim, H.-J., Brown, M.E., 2011. Phenology shifts at start vs. end of growing season in temperate vegetation over the Northern Hemisphere for the period 1982–2008. *Glob. Chang. Biol.* 17, 2385–2399. <https://doi.org/10.1111/j.1365-2486.2011.02397.x>.
- Jeong, S.-J., Medvigy, D., Sheviakova, E., Malyshev, S., 2012. Uncertainties in terrestrial carbon budgets related to spring phenology. *J. Geophys. Res. Biogeosciences* 117. <https://doi.org/10.1029/2011JG001868>.
- Jin, H., Eklundh, L., 2014. A physically based vegetation index for improved monitoring of plant phenology. *Remote Sens. Environ.* 152, 512–525. <https://doi.org/10.1016/j.rse.2014.07.010>.
- Jonsson, P., Eklundh, L., 2002. Seasonality extraction by function fitting to time-series of satellite sensor data. *IEEE Trans. Geosci. Remote Sens.* 40, 1824–1832. <https://doi.org/10.1109/TGRS.2002.802519>.
- Kato, S., Komiyama, A., 2002. Spatial and seasonal heterogeneity in understory light conditions caused by differential leaf flushing of deciduous overstory trees. *Ecol. Res.* 17, 687–693. <https://doi.org/10.1046/j.1440-1703.2002.00529.x>.
- Keenan, T.F., Richardson, A.D., 2015. The timing of autumn senescence is affected by the timing of spring phenology: implications for predictive models. *Glob. Chang. Biol.* 21, 2634–2641. <https://doi.org/10.1111/gcb.12890>.
- Klostner, S.T., Hufkens, K., Gray, J.M., Melaas, E., Sonnentag, O., Lavine, I., Mitchell, L., Norman, R., Friedl, M.A., Richardson, A.D., 2014. Evaluating remote sensing of deciduous forest phenology at multiple spatial scales using PhenoCam imagery. *Biogeosciences* 11, 4305–4320. <https://doi.org/10.5194/bg-11-4305-2014>.
- Kobayashi, H., Yunus, A.P., Nagai, S., Sugiura, K., Kim, Y., Van Dam, B., Nagano, H., Zona, D., Harazono, Y., Bret-Harte, M.S., Ichii, K., Ikawa, H., Iwata, H., Oechel, W.C., Ueyama, M., Suzuki, R., 2016. Latitudinal gradient of spruce forest understory and tundra phenology in Alaska as observed from satellite and ground-based data. *Remote Sens. Environ.* 177, 160–170. <https://doi.org/10.1016/j.rse.2016.02.020>.
- Laskin, D., Montagh, A., Nielsen, S., McDermid, G., 2016. Estimating Understory Temperatures Using MODIS LST in Mixed Cordilleran Forests. *Remote Sens.* 8, 658. <https://doi.org/10.3390/rs8080658>.
- Laskin, D.N., McDermid, G.J., Nielsen, S.E., Marshall, S.J., Roberts, D.R., Montagh, A., 2019. Advances in phenology are conserved across scale in present and future climates. *Nat. Clim. Chang.* 9, 419–425. <https://doi.org/10.1038/s41558-019-0454-4>.
- Leach, N., Coops, N.C., Obrknezev, N., 2019. Normalization method for multi-sensor high spatial and temporal resolution satellite imagery with radiometric inconsistencies. *Comput. Electron. Agric.* 164, 104893. <https://doi.org/10.1016/j.compag.2019.104893>.
- Liang, L., Schwartz, M.D., Fei, S., 2012. Photographic assessment of temperate forest understory phenology in relation to springtime meteorological drivers. *Int. J. Biometeorol.* 56, 343–355. <https://doi.org/10.1007/s00484-011-0438-1>.

- Liang, L., Schwartz, M.D., Fei, S., 2011. Validating satellite phenology through intensive ground observation and landscape scaling in a mixed seasonal forest. *Remote Sens. Environ.* 115, 143–157. <https://doi.org/10.1016/j.rse.2010.08.013>.
- Liang, L., Schwartz, M.D., Wang, Zhusoen, Gao, Feng, Schaaf, C.B., Tan, Bin, Morissette, J.T., Zhang, Xiaoyang, 2014. A cross comparison of spatiotemporally enhanced springtime phenological measurements from satellites and ground in a Northern U.S. Mixed Forest. *IEEE Trans. Geosci. Remote Sens.* 52, 7513–7526. <https://doi.org/10.1109/TGRS.2014.2313558>.
- Liu, Lingling, Liang, L., Schwartz, M.D., Donnelly, A., Wang, Z., Schaaf, C.B., Liu, Liangyun, 2015. Evaluating the potential of MODIS satellite data to track temporal dynamics of autumn phenology in a temperate mixed forest. *Remote Sens. Environ.* 160, 156–165. <https://doi.org/10.1016/j.rse.2015.01.011>.
- Locke, C.M., Anhalt-Depies, C.M., Frett, S., Stenglein, J.L., Cameron, S., Malleshappa, V., Peltier, T., Zuckerberg, B., Townsend, P.A., 2019. Managing a large citizen science project to monitor wildlife. *Wildl. Soc. Bull.* 43, 4–10. <https://doi.org/10.1002/wsb.943>.
- Mahall, B.E., Bormann, F.H., 1978. A quantitative description of the vegetative phenology of herbs in a northern hardwood forest. *Bot. Gaz.* 139, 467–481. <https://doi.org/10.1086/337022>.
- Melaas, E.K., Friedl, M.A., Richardson, A.D., 2016a. Multiscale modeling of spring phenology across Deciduous Forests in the Eastern United States. *Glob. Chang. Biol.* 22, 792–805. <https://doi.org/10.1111/gcb.13122>.
- Melaas, E.K., Friedl, M.A., Zhu, Z., 2013. Detecting interannual variation in deciduous broadleaf forest phenology using Landsat TM/ETM+ data. *Remote Sens. Environ.* 132, 176–185. <https://doi.org/10.1016/j.rse.2013.01.011>.
- Melaas, E.K., Sulla-Menashe, D., Gray, J.M., Black, T.A., Morin, T.H., Richardson, A.D., Friedl, M.A., 2016b. Multisite analysis of land surface phenology in North American temperate and boreal deciduous forests from Landsat. *Remote Sens. Environ.* 186, 452–464. <https://doi.org/10.1016/j.rse.2016.09.014>.
- Mishra, N., Haque, M., Leigh, L., Aaron, D., Helder, D., Markham, B., 2014. Radiometric Cross Calibration of Landsat 8 Operational Land Imager (OLI) and Landsat 7 Enhanced Thematic Mapper Plus (ETM+). *Remote Sens.* 6, 12619–12638. <https://doi.org/10.3390/rs61212619>.
- Monahan, W.B., Rosemarin, A., Gerst, K.L., Fischell, N.A., Ault, T., Schwartz, M.D., Gross, J.E., Weltzin, J.F., 2016. Climate change is advancing spring onset across the U.S. national park system. *Ecosphere* 7, e01465. <https://doi.org/10.1002/ecs2.1465>.
- Morin, X., Lechowicz, M.J., Augspurger, C., O'Keefe, J., Viner, D., Chuine, I., 2009. Leaf phenology in 22 North American tree species during the 21st century. *Glob. Chang. Biol.* 15, 961–975. <https://doi.org/10.1111/j.1365-2486.2008.01735.x>.
- Moody, A., Johnson, D.M., 2001. Land-surface phenologies from AVHRR using the discrete Fourier transform. *Remote Sens. Environ.* 75, 305–323. [https://doi.org/10.1016/S0034-4257\(00\)00175-9](https://doi.org/10.1016/S0034-4257(00)00175-9).
- Moore, C.E., Brown, T., Keenan, T.F., Duursma, R.A., van Dijk, A.I.J.M., Beringer, J., Culvenor, D., Evans, B., Huete, A., Hutley, L.B., Maier, S., Restrepo-Coupe, N., Sonnentag, O., Specht, A., Taylor, J.R., van Gorsel, E., Liddell, M.J., 2016. Reviews and syntheses: Australian vegetation phenology: new insights from satellite remote sensing and digital repeat photography. *Biogeosciences* 13, 5085–5102. <https://doi.org/10.5194/bg-13-5085-2016>.
- Myinen, R.B., Keeling, C.D., Tucker, C.J., Asrar, G., Nemani, R.R., 1997. Increased plant growth in the northern high latitudes from 1981 to 1991. *Nature* 386, 698–702. <https://doi.org/10.1038/386698a0>.
- Nasahara, K.N., Nagai, S., 2015. Review: Development of an in situ observation network for terrestrial ecological remote sensing: the Phenological Eyes Network (PEN). *Ecol. Res.* 30, 211–223. <https://doi.org/10.1007/s11284-014-1239-x>.
- Nijland, W., Bolton, D.K., Coops, N.C., Stenhouse, G., 2016. Imaging phenology: scaling from camera plots to landscapes. *Remote Sens. Environ.* 177, 13–20. <https://doi.org/10.1016/j.rse.2016.02.018>.
- Pacifici, K., Reich, B.J., Miller, D.A.W., Gardner, B., Stauffer, G., Singh, S., McKerrow, A., Collazo, J.A., 2017. Integrating multiple data sources in species distribution modeling: a framework for data fusion*. *Ecology* 98, 840–850. <https://doi.org/10.1002/ecy.1710>.
- Pahlevan, N., Chittimalli, S.K., Balasubramanian, S.V., Vellucci, V., 2019. Sentinel-2/Landsat-8 product consistency and implications for monitoring aquatic systems. *Remote Sens. Environ.* 220, 19–29. <https://doi.org/10.1016/j.rse.2018.10.027>.
- Penuelas, J., 2001. PHENOLOGY: Responses to a warming world. *Science* (80-) 294, 793–795. <https://doi.org/10.1126/science.1066860>.
- Penuelas, J., Rutishauser, T., Filella, I., 2009. Phenology feedbacks on climate change. *Science* (80-) 324, 887–888. <https://doi.org/10.1126/science.1173004>.
- Piao, S., Liu, Q., Chen, A., Janssens, I.A., Fu, Y., Dai, J., Liu, L., Lian, X., Shen, M., Zhu, X., 2019. Plant phenology and global climate change: Current progresses and challenges. *Glob. Chang. Biol.* 25, 1922–1940. <https://doi.org/10.1111/gcb.14619>.
- Prevéry, J.S., Parker, L.E., Harrington, C.A., Lamb, C.T., Proctor, M.F., 2020. Climate change shifts in habitat suitability and phenology of huckleberry (*Vaccinium membranaceum*). *Agric. For. Meteorol.* 280, 107803. <https://doi.org/10.1016/j.agrformet.2019.107803>.
- Reed, B.C., Brown, J.F., VanderZee, D., Loveland, T.R., Merchant, J.W., Ohlen, D.O., 1994. Measuring phenological variability from satellite imagery. *J. Veg. Sci.* 5, 703–714. <https://doi.org/10.2307/3235884>.
- Richardson, Andrew D., Hufkens, K., Milliman, T., Aubrecht, D.M., Chen, M., Gray, J.M., Johnston, M.R., Keenan, T.F., Klosterman, S.T., Kosmala, M., Melaas, E.K., Friedl, M.A., Frolking, S., 2018a. Tracking vegetation phenology across diverse North American biomes using PhenoCam imagery. *Sci. Data* 5, 180028. <https://doi.org/10.1038/sdata.2018.28>.
- Richardson, Andrew D., Hufkens, K., Milliman, T., Frolking, S., 2018b. Intercomparison of phenological transition dates derived from the PhenoCam Dataset V1.0 and MODIS satellite remote sensing. *Sci. Rep.* 8, 1–12. <https://doi.org/10.1038/s41598-018-23804-6>.
- Richardson, A.D., Keenan, T.F., Migliavacca, M., Ryu, Y., Sonnentag, O., Toomey, M., 2013. Climate change, phenology, and phenological control of vegetation feedbacks to the climate system. *Agric. For. Meteorol.* 169, 156–173. <https://doi.org/10.1016/j.agrformet.2012.09.012>.
- Richardson, A.J., O'Keefe, J.F., 2009. Phenological differences between understory and overstory : A case study using the long-term Harvard forest records. In: Noormets, A. (Ed.), *Phenology of Ecosystem Processes*. Springer, New York, pp. 87–117.
- Roy, D.P., Ju, J., Lewis, P., Schaaf, C., Gao, F., Hansen, M., Lindquist, E., 2008. Multi-temporal MODIS-Landsat data fusion for relative radiometric normalization, gap filling, and prediction of Landsat data. *Remote Sens. Environ.* 112, 3112–3130. <https://doi.org/10.1016/j.rse.2008.03.009>.
- Sadeh, Y., Zhu, X., Dunkerley, D., Walker, J.P., Zhang, Y., Rosenstein, O., Manivasagam, V.S., Chen, K., 2021. Fusion of Sentinel-2 and PlanetScope time-series data into daily 3 m surface reflectance and wheat LAI monitoring. *Int. J. Appl. Earth Obs. Geoinf.* 96, 102260. <https://doi.org/10.1016/j.jag.2020.102260>.
- Schaaf, C.B., Gao, F., Strahler, A.H., Lucht, W., Li, X., Tsang, T., Strugnell, N.C., Zhang, X., Jin, Y., Müller, J., Lewis, P., Barnsley, M., Hobson, P., Disney, M., Roberts, G., Dunderdale, M., Doll, C., Robert, P., Hu, B., Liang, S., Privette, J.L., Q'Roy, J.D., 2002. First operational BRDF, albedo nadir reflectance products from MODIS. *Remote Sens. Environ.* 83, 135–148.
- Sakamoto, T., Yokozawa, M., Toritani, H., Shibayama, M., Ishitsuka, N., Ohno, H., 2005. A crop phenology detection method using time-series MODIS data. *Remote Sens. Environ.* 96, 366–374. <https://doi.org/10.1016/j.rse.2005.03.008>.
- Salas, E.A.L., 2020. Waveform LiDAR concepts and applications for potential vegetation phenology monitoring and modeling: a comprehensive review. *Geo-spatial Inf. Sci.* 1–22. <https://doi.org/10.1080/10095020.2020.1761763>.
- Schwartz, M.D., Ahas, R., Aasa, A., 2006. Onset of spring starting earlier across the Northern Hemisphere. *Glob. Chang. Biol.* 12, 343–351. <https://doi.org/10.1111/j.1365-2486.2005.01097.x>.
- Schwartz, M.D., Betancourt, J.L., Weltzin, J.F., 2012. From Caprio's lilacs to the USA National Phenology Network. *Front. Ecol. Environ.* 10, 324–327. <https://doi.org/10.1890/110281>.
- Schwartz, M.D., Hanes, J.M., 2010. Intercomparing multiple measures of the onset of spring in eastern North America. *Int. J. Climatol.* 30, 1614–1626. <https://doi.org/10.1002/joc.2008>.
- Serbin, S.P., Kucharik, C.J., 2009. Spatiotemporal Mapping of Temperature and Precipitation for the Development of a Multidecadal Climatic Dataset for Wisconsin. *J. Appl. Meteorol. Climatol.* 48, 742–757. <https://doi.org/10.1175/2008JAMC1986.1>.
- Sirén, A.P.K., Somos-Valenzuela, M., Callahan, C., Kilborn, J.R., Duclos, T., Tragert, C., Morelli, T.L., 2018. Looking beyond wildlife: using remote cameras to evaluate accuracy of gridded snow data. *Remote Sens. Ecol. Conserv.* 4, 375–386. <https://doi.org/10.1002/rse.285>.
- Sparling, J.H., 1967. Assimilation rates of some woodland herbs in Ontario. *Bot. Gaz.* 128, 160–168.
- St. Peter, J., Hogland, J., Hebblewhite, M., Hurley, M., Hupp, N., Proffitt, K., 2018. Linking Phenological Indices from Digital Cameras in Idaho and Montana to MODIS NDVI. *Remote Sens.* 10, 1612. <https://doi.org/10.3390/rs10101612>.
- Steenweg, R., Hebblewhite, M., Kays, R., Ahumada, J., Fisher, J.T., Burton, C., Townsend, S.E., Carbone, C., Rowcliffe, J.M., Whittington, J., Brodie, J., Royle, J.A., Switalski, A., Clevenger, A.P., Heim, N., Rich, L.N., 2017. Scaling-up camera traps: monitoring the planet's biodiversity with networks of remote sensors. *Front. Ecol. Environ.* 15, 26–34. <https://doi.org/10.1002/fee.1448>.
- Townsend, P.A., Clare, J., Liu, N., Stenglein, J.L., Anhalt-Depies, C., Deelen, T.R., Van, Gilbert, N.A., Singh, A., Martin, K.J., Zuckerberg, B., 2020. Integrating remote sensing and jurisdictional observation networks to improve the resolution of ecological management (revision in review). *Ecol. Appl. bioRxiv* 10.1101/2020.06.08.140488.
- Uemura, S., 1994. Patterns of leaf phenology in forest understory. *Can. J. Bot.* 72, 409–414. <https://doi.org/10.1139/b94-055>.
- van Vliet, A.J.H., de Groot, R.S., Bellens, Y., Braun, P., Bruegger, R., Bruns, E., Clevers, J., Estreguil, C., Flechsig, M., Jeanneret, F., Maggi, M., Martens, P., Menne, B., Menzel, A., Sparks, T., 2003. The European Phenology Network. *Int. J. Biometeorol.* 47, 202–212. <https://doi.org/10.1007/s00484-003-0174-2>.
- Vartanian, M., Nijland, W., Coops, N.C., Bater, C., Wulder, M.A., Stenhouse, G., 2014. Assessing the impact of field of view on monitoring understory and overstory phenology using digital repeat photography. *Can. J. Remote Sens.* 40, 85–91. <https://doi.org/10.1080/07038992.2014.930308>.
- Vrieling, A., Meroni, M., Darvishzadeh, R., Skidmore, A.K., Wang, T., Zurita-Milla, R., Oosterbeek, K., O'Connor, B., Paganini, M., 2018. Vegetation phenology from Sentinel-2 and field cameras for a Dutch barrier island. *Remote Sens. Environ.* 215, 517–529. <https://doi.org/10.1016/j.rse.2018.03.014>.
- Walker, J.J., de Beurs, K.M., Wynne, R.H., Gao, F., 2012. Evaluation of Landsat and MODIS data fusion products for analysis of dryland forest phenology. *Remote Sens. Environ.* 117, 381–393. <https://doi.org/10.1016/j.rse.2011.10.014>.
- Walther, G.R., Post, E., Convey, P., Menzel, A., Parmesan, C., Beebee, T.J.C., Fromentin, J.M., Hoegh-Guldberg, O., Bairlein, F., 2002. Ecological responses to recent climate change. *Nature* 416, 389–395. <https://doi.org/10.1038/416389a>.
- Wang, Q., Blackburn, G.A., Onojeghuo, A.O., Dash, J., Zhou, L., Zhang, Y., Atkinson, P.M., 2017. Fusion of Landsat 8 OLI and Sentinel-2 MSI Data. *IEEE Trans. Geosci. Remote Sens.* 55, 3885–3899. <https://doi.org/10.1109/TGRS.2017.2683444>.
- Wang, Q., Shi, W., Li, Z., Atkinson, P.M., 2016. Fusion of Sentinel-2 images. *Remote Sens. Environ.* 187, 241–252. <https://doi.org/10.1016/j.rse.2016.10.030>.

- Wegmueller, S., Leach, N., Townsend, P.A., n.d. LOESS radiometric correction for contiguous scenes (LORACCS): Improving the consistency of radiometry in high-resolution satellite image mosaics. *Int. J. Appl. Earth Obs. Geoinf.*
- White, K., Pontius, J., Schaberg, P., 2014. Remote sensing of spring phenology in northeastern forests: A comparison of methods, field metrics and sources of uncertainty. *Remote Sens. Environ.* 148, 97–107. <https://doi.org/10.1016/j.rse.2014.03.017>.
- White, M.A., De Beurs, K.M., Didan, K., Inouye, D.W., Richardson, A.D., Jensen, O.P., O'keefe, J., Zhang, G., Nemani, R.R., Van Leeuwen, W.J.D., Brown, J.F., De Wit, A., Schaepman, M., Lin, X., Dettinger, M., Bailey, A.S., Kimball, J., Schwartz, M.D., Baldocchi, D.D., Lee, J.T., Lauenroth, W.K., 2009. Intercomparison, interpretation, and assessment of spring phenology in North America estimated from remote sensing for 1982–2006. *Glob. Chang. Biol.* 15, 2335–2359. [10.1111/j.1365-2486.2009.01910.x](https://doi.org/10.1111/j.1365-2486.2009.01910.x).
- Wingate, L., Ogee, J., Cremonese, E., Filippa, G., Mizunuma, T., Migliavacca, M., Moisy, C., Wilkinson, M., Moureaux, C., Wohlfahrt, G., Hammerle, A., Hörtnagl, L., Gimeno, C., Porcar-Castell, A., Galvagno, M., Nakajin, T., Morison, J., Kolle, O., Knöhl, A., Kutsch, W., Kolaric, P., Nikinmaa, E., Ibrom, A., Gielen, B., Eugster, W., Balzarolo, M., Papale, D., Klumpp, K., Köstner, B., Grünwald, T., Joffre, R., Ourcival, J.-M., Hellstrom, M., Lindroth, A., Charles, G., Longdoz, B., Genty, B., Levula, J., Heinesch, B., Sprintsin, M., Yakir, D., Manise, T., Guyon, D., Ahrendts, H., Plaza-Aguilar, A., Guan, J.H., Grace, J., 2015. Interpreting canopy development and physiology using the EUROPEn camera network at flux sites. *Biogeosci. Discuss.* 12, 7979–8034. <https://doi.org/10.5194/bgd-12-7979-2015>.
- Wolkovich, E.M., Cook, B.I., Allen, J.M., Crimmins, T.M., Betancourt, J.L., Travers, S.E., Pau, S., Regetz, J., Davies, T.J., Kraft, N.J.B., Ault, T.R., Bolmgren, K., Mazer, S.J., McCabe, G.J., McGill, B.J., Parmesan, C., Salamin, N., Schwartz, M.D., Cleland, E.E., 2012. Warming experiments underpredict plant phenological responses to climate change. *Nature* 485, 494–497. <https://doi.org/10.1038/nature11014>.
- Yu, R., Schwartz, M.D., Donnelly, A., Liang, L., 2016. An observation-based progression modeling approach to spring and autumn deciduous tree phenology. *Int. J. Biometeorol.* 60, 335–349. <https://doi.org/10.1007/s00484-015-1031-9>.
- Zhang, H.K., Roy, D.P., Yan, L., Li, Z., Huang, H., Vermote, E., Skakun, S., Roger, J.-C., 2018. Characterization of Sentinel-2A and Landsat-8 top of atmosphere, surface, and nadir BRDF adjusted reflectance and NDVI differences. *Remote Sens. Environ.* 215, 482–494. <https://doi.org/10.1016/j.rse.2018.04.031>.
- Zhang, X., Friedl, M.A., Schaaf, C.B., Strahler, A.H., Hodges, J.C.F., Gao, F., Reed, B.C., Huete, A., 2003. Monitoring vegetation phenology using MODIS. *Remote Sens. Environ.* 84, 471–475. [https://doi.org/10.1016/S0034-4257\(02\)00135-9](https://doi.org/10.1016/S0034-4257(02)00135-9).
- Zhang, X., Wang, J., Gao, F., Liu, Y., Schaaf, C., Friedl, M., Yu, Y., Jayavelu, S., Gray, J., Liu, L., Yan, D., Henebry, G.M., 2017. Exploration of scaling effects on coarse resolution land surface phenology. *Remote Sens. Environ.* 190, 318–330. <https://doi.org/10.1016/j.rse.2017.01.001>.
- Zheng, Z., Zhu, W., 2017. Uncertainty of Remote Sensing Data in Monitoring Vegetation Phenology: A Comparison of MODIS C5 and C6 Vegetation Index Products on the Tibetan Plateau. *Remote Sens.* 9, 1288. <https://doi.org/10.3390/rs9121288>.